ABSTRACT

DUGAN, SEAN PATRICK-MICHAEL. On the Design, Modeling, and Control of a Hybrid Pump System for Dynamic Pressurization of Explanted Mammalian Hearts. (Under the direction of Dr. Gregory D. Buckner.)

A hybrid electromechanical pump system is proposed to mimic left ventricular blood pressure in a living mammalian heart. The system consists of a gear pump and voice coil actuated diaphragm (VCAD) pump connected in parallel. By combining a high-capacity, low-bandwidth gear pump with a low-capacity, high-bandwidth VCAD pump, the advantages of both can be realized, resulting in an economical high-bandwidth pumping system that may be used with animal hearts of arbitrary size. Mathematical models are developed to describe the system dynamics and develop a digital controller. Experimental results are also presented.

On the Design, Modeling, and Control of a Hybrid Pump System for Dynamic Pressurization of Explanted Mammalian Hearts

By

Sean Patrick-Michael Dugan

A Thesis submitted to the Graduate Faculty of
North Carolina State University
in partial fulfillment of the
requirements for the degree of
Master of Science

Mechanical Engineering

Raleigh, North Carolina
2007

APPROVED BY:

Dr. Gregory D. Buckner (Chair of Advisory Committee)	Dr. Denis R. Cormier
Dr. Andre P. Mazzoleni	Dr. Larry Silverberg

Dedication

This thesis is dedicated to my wife Sandra Dugan, and my mom Bettina Stoll-Dugan.

Biography

Sean Dugan was born in Lincoln, Nebraska, and graduated from Lincoln High School. He earned a Bachelor of Science in Mechanical Engineering from the University of Nebraska, and currently resides in Germany.

Acknowledgments

First of all, I would like to thank Dr. Gregory Buckner. Without his encouragement and support, this thesis would have never come to pass.

Thanks also go to BEI KIMCO for providing a voice coil actuator for the VCAD pump prototype, Shaphan Jernigan for all of his help in the lab, Skip Richardson for his patience and expertise during the construction of the prototype, and, finally, Judy Cline for helping me navigate through all of the paperwork.

Contents

List of Tables

List of Figures

1 Introduction

Cardiovascular disease (CVD) is by far the leading cause of death in modern Western countries, accounting for four million deaths per year in Europe [2] and nearly one million deaths per year in the US [3]. Common surgical treatments for CVD include coronary artery bypass grafts, valve replacement and valve repair. These and other surgical procedures traditionally require "open" access to the thoracic cage, usually by splitting and retracting the sternum (median sternotomy). "Open heart" surgery provides direct visualization and access, enabling surgeons to use their hands in an effective manner.

While widely used, open heart procedures have serious drawbacks. Median sternotomy is frequently associated with tissue trauma, chronic post-surgical pain, longer recovery times, and increased risk of infection. Many of these drawbacks may be avoided by employing minimally invasive surgery (MIS) or minimally invasive robot-assisted (MIRA) procedures [4]. MIS procedures utilize endoscopic or laparoscopic instruments (Fig.1) introduced through small incisions, eliminating the need for median sternotomy. Surgical tasks such as cutting, knot tying and inspection may be performed through the same incision using remotely actuated instruments. MIRA methods take MIS one step further by employing teleoperated manipulators along with stereoptic feedback to assist the surgeon.

The principle drawback of MIS/MIRA procedures is that surgical time is often longer than that of traditional methods, with no documented reduction in health care costs. Exacerbating this problem is the limited pool of surgeons

trained in MIS methods. Endoscopic techniques require highly experienced surgeons who are capable of using these instruments precisely. According to Bailey and Flowers [5], "The skills necessary to perform safe laparoscopic or thoracoscopic surgery have not been routinely taught during most surgical training programs."

The focus of this research is the development and demonstration of an economical and flexible pumping system for dynamic pressurization of an explanted mammalian heart. This electromechanical system will enable the development, training, and refinement of surgical procedures for minimally-invasive cardiac surgery, specifically mitral valve repair.

Figure 1: Typical laparoscopic instruments (www.aesculapusa.com)

1.1 Pressurization of the left ventricle

A schematic of the human circulatory system indicating the relative position of the mitral valve is shown in Fig.2.

To activate the mitral valve of a denervated heart, it is necessary to generate a periodic pressure differential across the valve using some sort of pumping system. While systems designed to achieve similar tasks have been proposed, all use either a linear piston/diaphragm pump [6, 7, 8] or a rotary pump [9]. Systems that depend exclusively on one type of pump suffer from

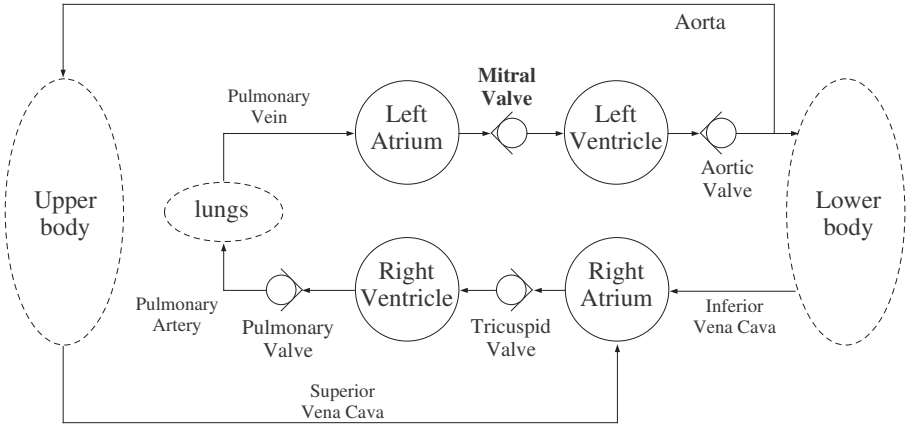

Figure 2: The mammalian circulatory system

distinct disadvantages. For example, a system based on a diaphragm pump actuated by a high-bandwidth low-hysteresis actuator, such as a voice coil, is able to control pressure in the high frequency range but has too low of a stroke volume to pressurize larger animal hearts. Also, performing static valve sufficiency tests (maintaining pressure at a specific level to measure leakage) is not possible.

To increase the stroke, a pump system design may incorporate a piston pump with a large-stroke actuator such as a pneumatic piston or a power screw. However, due to the high stiction and hysteresis of a piston, such a system will have inherently poor bandwidth (and may leak). Further, any improvement in stroke volume will be limited by the volume of the piston.

Rotary pumps such as centrifugal or gear pumps, which have effectively infinite stroke volumes, may be used to pressurize ventricles of arbitrary compliance. These pumps, however, suffer from bandwidth limitations due to non-reversibility (centrifugal pumps), or significant stiction problems (centrifugal and gear pumps).

The ideal solution is to form a hybrid pump system by connecting in parallel a high-bandwidth, low-flow voice coil actuated diaphragm pump (VCAD pump) with a reversible, low-bandwidth, high-flow gear pump. Such a hybrid system combines the positive attributes of both the VCAD and gear pumps and results in an economical high-bandwidth pumping system that may be used with animal hearts of arbitrary size.

1.2 Thesis overview

This thesis discusses the design, modeling, and experimental demonstration of a hybrid pumping system for explanted mammalian hearts using a gear and VCAD pump connected in parallel.

Section 2 describes the overall architecture of the proposed system and explains the basic operating procedure.

Section 3 develops from elementary principles the governing equations of the elements that comprise the system. Nonlinear multi-physics models (electrical, mechanical, and hydraulic) are then formulated to describe the dynamics of the different stages.

Section 4 briefly describes the physical design requirements of the system, including maximum flow rate and pressure. Also, an economical design is proposed for the actual construction of a pump frame and bearing system.

Section 5 discusses the design of a microcontroller-based circuit to control the system. The design includes an instrumentation amplifier to condition a pressure transducer signal, as well as an H-bridge circuit to provide power to the pumps.

In Section 6, discrete PD and PID controllers are derived.

Section 7 discusses experiments performed to test the system.

Finally, Section 8 reviews the topics discussed in this thesis and draws conclusions from the experimental results.

2 System architecture and operation

The proposed system architecture is depicted in Fig.3. The system consists of a gear pump, a VCAD pump, and a fluid reservoir. The gear pump provides low-bandwidth, high-volume fluid transfer, pushing fluid out of the reservoir, where it joins with output from the VCAD. The VCAD provides high-bandwidth, limited flow rate control of the pumping operation. The combined output flows into the explanted ventricle through the aortic valve. The fluid reservoir maintains the minimum desired system pressure and provides the hydraulic capacitance needed for ventricular filling during the diastolic phase.

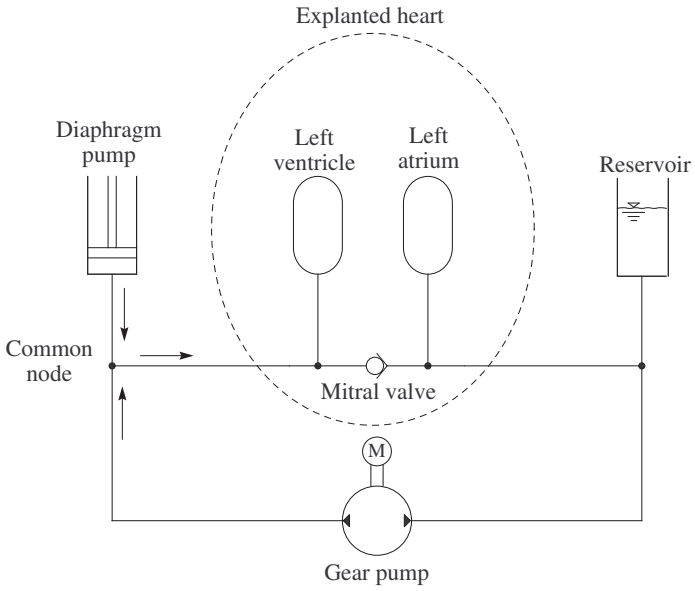

Figure 3: Architecture for the dual pump system

Due to the presence of the mitral valve, the periodic pumping process can be divided into two stages. The first stage, Stage I, equivalent to dias-

tole, consists of the gear pump moving fluid out of the ventricle and into the reservoir. This action creates a negative ventricular-atrial pressure differential ($p_v - p_a$) causing the mitral valve to open.

During Stage II, equivalent to systole, the gear pump is reversed causing a positive ventricular-atrial pressure difference which forces the mitral valve to close. The pressure within the ventricle (p_v) then begins to rise.

The gear pump enables low-bandwidth tracking of a predetermined pressure trajectory within the ventricle, which varies from the diastolic pressure p_{dia} to the systolic pressure p_{sys}. The gear pump alone, however, lacks the bandwidth to control the high frequency components of the system response. Fig.4 demonstrates, hypothetically, how combining a VCAD pump with the gear pump increases the effective bandwidth of the system.

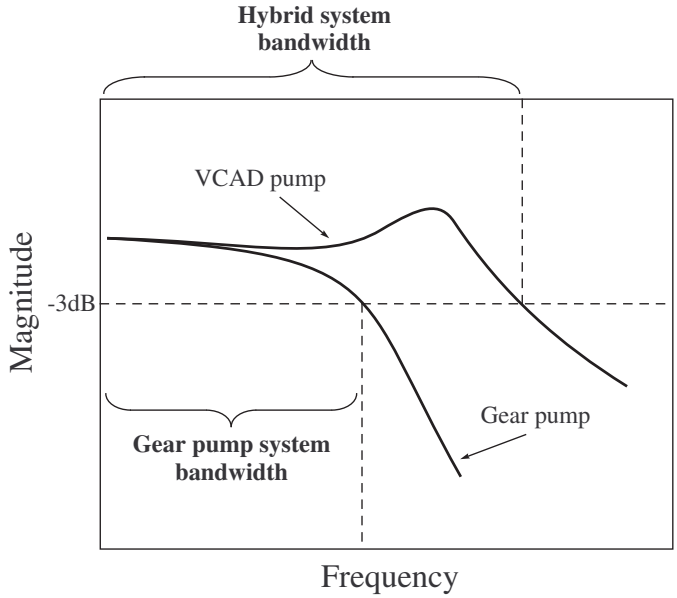

Figure 4: Hypothetical Bode plot of the hybrid system.

3 System modeling

To derive an overall model of the system, it is first necessary to determine the governing equations of the elements.

3.1 Element models

Fluid flow through hydraulic systems, like the proposed device and animal vascular systems, are often modeled using analogous electrical systems. As shown in [10] and [11], flow through a conduit like a vein or artery is modeled using a series-connected resistor and inductor along with a capacitor connected to ground. The resistor accounts for the pressure drop due to fluid friction effects, while the inductor relates the applied pressure to the inertial properties of the fluid. The capacitor models the ability of a conduit to expand under pressure.

Fig.5 contains a table of the schematic hydraulic symbols used in this paper, and their electrical analogs.

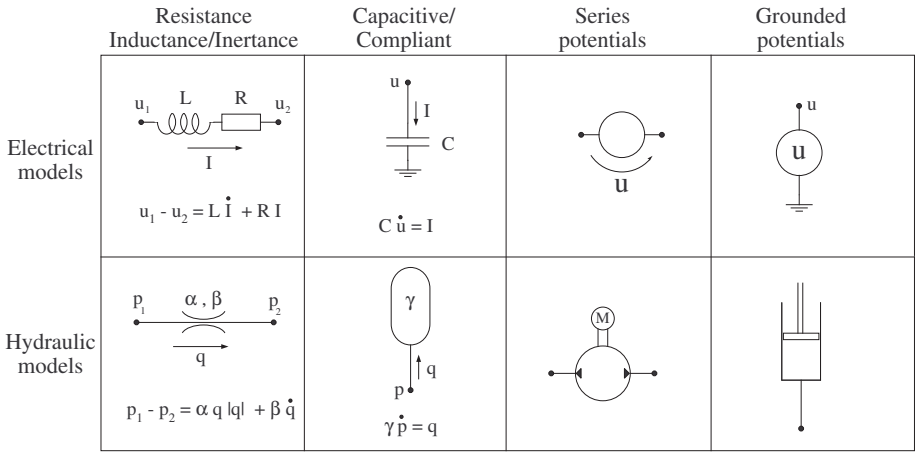

Figure 5: Schematic symbols

Essentially, there are three element types in the system: compliant (heart chambers and reservoirs, analogous to electrical capacitors), resistive (tubes and connectors), and motive (the rotary and linear pumps). A fourth "element" (more like a property) of the system is the inertance of the fluid, which is dependent upon the density of the fluid and the size and shape of the conduit (analogous to electrical inductance).

3.1.1 Pressure drop across conduits

To derive the governing equation of the pressure drop $(p_1 - p_2)$ along a length of tubing, the cylindrical fluid element of Fig.6 is considered. By Newton's Second Law, the sum of the forces applied to the element is related to the acceleration of the element. Excluding pressure changes due to gravity (changes in elevation),

$$pdA - (p + \frac{\partial p}{\partial x}dx)\ dA - \tau D\pi\ dx = dm\ \ddot{x} \tag{3.1}$$

Expanding the second term on the left side and dividing through by $dx\ dA$,

$$-\frac{\partial p}{\partial x} - \tau D\pi \frac{dx}{dxdA} = \frac{dm}{dxdA}\ddot{x} \tag{3.2}$$

Noting that $\mathrm{D}\pi = \frac{4dA}{D}$ and $\frac{dm}{dxdA} = \rho$,

$$-\frac{\partial p}{\partial x} - \frac{4\tau}{D} = \rho\ddot{x} \tag{3.3}$$

If the fluid velocity, $\dot{x}$, is replaced by $\frac{q}{A}$ (the volumetric flow rate, q in $\frac{m^3}{s}$, divided by the cross sectional area A of the conduit), the partial derivative

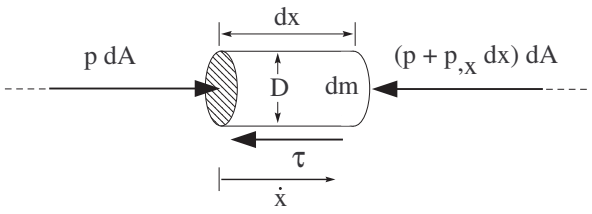

Figure 6: Deriving the relation between pressure drop and fluid acceleration along a streamline. ($p_{,x} = \frac{\partial p}{\partial x}$)

with $\frac{p_2 - p_1}{L}$, (L is the length of the segment, and p_i is the average pressure across section i), and multiply through by L, we have

$$p_1 - p_2 = \frac{4\tau L}{D} + \frac{\rho L}{A}\dot{q} \tag{3.4}$$

The shear force may be estimated using the empirical correlation

$$\tau = \frac{1}{8} f \rho v \left| v \right| = \frac{1}{8A^2} f \rho q \left| q \right| \tag{3.5}$$

where f is the Darcy-Weisbach friction factor[12]. Substituting Eq.3.5 into Eq.3.4

$$p_1 - p_2 = \alpha q \left| q \right| + \beta \dot{q} \tag{3.6a}$$

$$\alpha := \frac{L f \rho}{2 D A^2} \tag{3.6b}$$

$$\beta := \frac{\rho L}{A} \tag{3.6c}$$

This result agrees with that derived in [12] and the lumped parameter term for β given without justification in [13].

3.1.2 Pressure at the entrance of compliant elements

The ventricle and atrium of the heart, as well as the fluid reservoir, may be treated as simple capacitors connected between the fluid source and "ground" (here, atmospheric pressure).

The pressure at the entrance of the compliant element is given by

$$p = \int_0^t \frac{1}{\gamma} q dt = \frac{V}{\gamma} \tag{3.7}$$

The term γ is the compliance, which depends on gravity and the elastic and geometric properties of the vessel. For the purpose of this paper, γ will be assumed constant (as it is assumed so in the literature, for example, [14]). In the case of an open, straight sided vessel of fluid surface area A, $\gamma = \frac{A}{\rho g}$, which can be easily verified.

The term V may be viewed as the "excess volume" of fluid inside of the element that causes it to expand beyond its normal relaxed volume.

3.1.3 Elastic diaphragm pump model

The general design of the diaphragm pump consists of a simple compliant element, such as a suction cup, that is deformed by a voice coil actuator.

The pump diaphragm may deform in two ways: it may either stretch or bend. When the diaphragm is deflected by a force F, as depicted in Fig.7, it essentially "rolls" inward to accommodate the deflection of the point of application of the force. The resistance to bending is represented by an axial stiffness constant k. Due to the elasticity of the diaphragm material, the pump diaphragm has a nonzero compliance, γ_e, which allows it to strain

tangentially to the diaphragm surface. When the pressure at the pump outlet is non-zero (bottom diagram of Fig.7), the amount of fluid ejected is reduced by an amount $V_r = \gamma_e p_p$, where p_p is the pressure inside of the pump (which is assumed uniform).

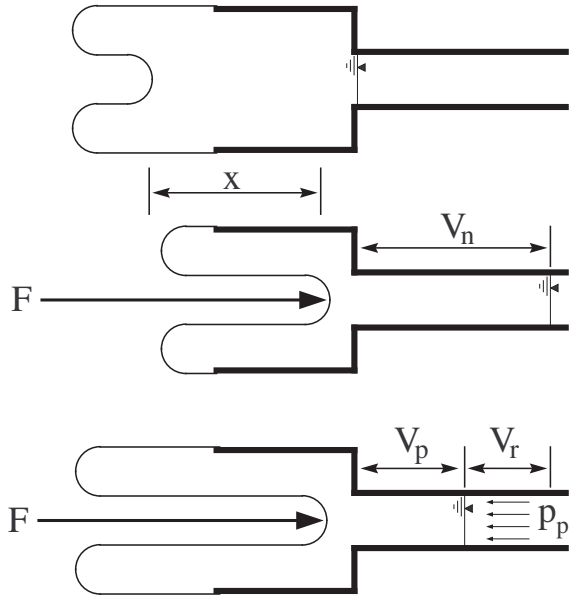

Figure 7: Elastic model of a diaphragm pump. The top diagram represents the pump in the undeformed state. The middle diagram represents a pump with no outlet load, or a pump with a diaphragm of zero compliance; in either case the diaphragms of both the top and middle figures have the same area. The bottom figure represents a pump with a non-zero compliance under load; the diaphragm has stretched.

For a pump with with zero outlet pressure (see the middle of Fig.7), if the point of application of a force F is displaced by a distance x, fluid of volume V_n is ejected from the pump. The ratio of V_n to x defines the parameter A

$$A(x) := \frac{V_n}{x} \tag{3.8}$$

This parameter, which may be thought of as a generalized pump piston "area", must be determined experimentally for various x. For small deflections, A may be assumed constant.

Schematically, the complete pump is modeled as massless piston of area A connected to a damper and spring of damping c and stiffness k, respectively; a simple compliant element γ_e is connected in parallel with the piston to account for the elasticity of the vessel. See Fig.8.

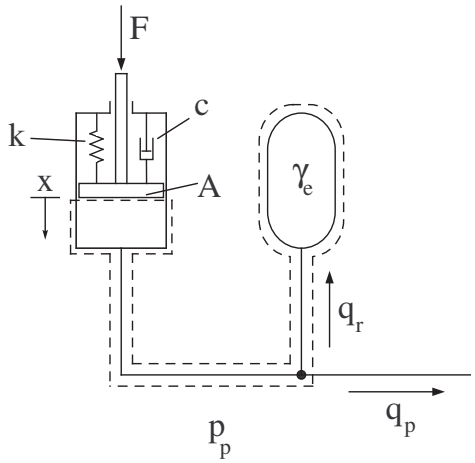

Figure 8: Lumped parameter model of the diaphragm pump. The pressure within the volume denoted by the dashed line is p_p and is uniform throughout.

The complete VCAD model is shown in Fig.9. The pressure p_d is the discharge pressure at the outlet of the pump. The parameters α and β are the fluid resistance and inertance of the pump outlet. These parameters may be lumped with corresponding parameters of the conduit connecting the pump to its target, while the discharge pressure may be considered to be the outlet of the conduit at the target.

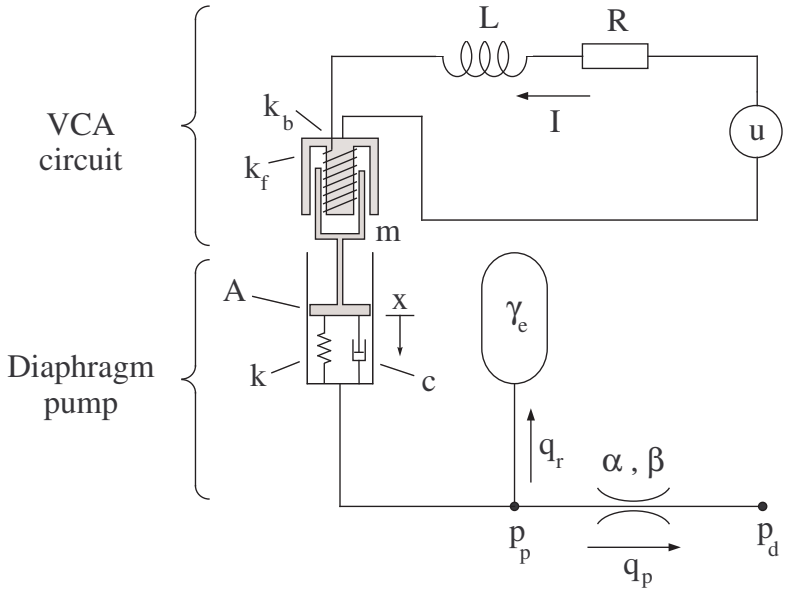

Figure 9: Lumped parameter model of the VCAD pump system

Assuming the fluid is incompressible, we have

$$V_n = Ax = V_r + V_p \tag{3.9}$$

where V_p is the fluid ejected from the pump under load.

Differentiating once, substituting $\dot{V}_r = q_r = \gamma_e \dot{p}_p$ and $\dot{V}_p = q_p$, and finally solving for $\dot{p}_p$

$$\dot{p}_p = \frac{A}{\gamma_e}\dot{x} - \frac{1}{\gamma_e}q_p \tag{3.10}$$

The pressure drop as the fluid leaves the pump is

$$p_p - p_d = \alpha q_p |q_p| + \beta \dot{q}_p \tag{3.11}$$

Differentiating once, solving for $\ddot{q}_p$, and substituting Eq.3.10 into the result

$$\ddot{q}_p = \frac{A}{\beta\gamma_e}\dot{x} - \frac{1}{\beta\gamma_e}q_p - \frac{1}{\beta}\dot{p}_d - \frac{2\alpha}{\beta}|q_p|\dot{q}_p \tag{3.12}$$

The electrical circuit for the VCA consists of a series connected voltage source, inductor, resistor, and back EMF[1] source[15]. The back EMF, u_b, is dependent on the speed of the VCA "mover", $\dot{x}$. Within a limited operating range, the back EMF is given by

$$u_b = k_b\dot{x} \tag{3.13}$$

Applying Kirchoff's voltage law, the equation governing the dynamics of the circuit is

$$L\dot{I} + RI + k_b\dot{x} = u \tag{3.14}$$

Because the inductance of a typical VCA is only a few mH [15], and may thus dropped, the equation becomes

$$I = -\frac{k_b}{R}\dot{x} + \frac{1}{R}u \tag{3.15}$$

The force F_a generated by the VCA is dependent on the circuit current. Also within a limited operating range, the force is given by

$$F_a = k_f I = -\frac{k_b k_f}{R}\dot{x} + \frac{k_f}{R}u \tag{3.16}$$

[1]Electro-motive force.

Since the mover of the actuator is rigidly connected to the diaphragm, the mechanical properties of the two are lumped together. Modeling the combined assembly as a 2^{nd} order mass-spring-damper

$$m\ddot{x} + c\dot{x} + kx = F_a - Ap_p \tag{3.17}$$

Substituting Eq.3.16 and solving for $\ddot{x}$

$$\ddot{x} = -\left(\frac{c}{m} + \frac{k_b k_f}{mR}\right)\dot{x} - \frac{k}{m}x - \frac{A}{m}p_p + \frac{k_f}{mR}u \tag{3.18}$$

Depending on the nature of the outlet load, Eqs.3.10, 3.12, and 3.18, may be used to form the state equations of the linear pump.

3.1.4 Gear pump model

A gear pump was selected for use in this design because it generates high output, is compact, and is inexpensive.

Fig.10 shows a simple diagram of an external gear pump of the type used. The pump consists of two enmeshed spur gears inside a sealed housing; one gear is driven (in this case directly) by an external DC motor. During operation, fluid is trapped between the teeth of the gears and the inside wall of the housing and is transported by the rotation of the gear from the suction (s) port to the discharge (d) port.

Gear pumps may be considered infinitely long positive displacement pumps, so like the diaphragm pump, we may use a simple piston (with modification) to develop a model. The model consists of a piston driven by a power screw, which in turn is driven by the standard no-inductance DC motor.

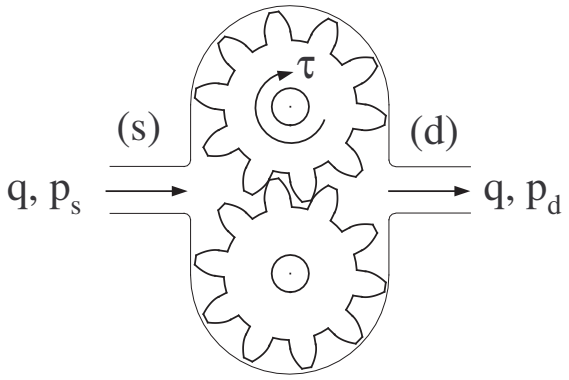

Figure 10: Schematic of a basic external-type gear pump

If we make the cylinder in which the piston moves, as well as the power screw which drives it, infinitely long, we have the "perpetual power screw" model of the gear pump (Fig.11). The resulting model may be understood by considering the following points:

1. The piston and power screw have no mass or friction. All inertial and damping properties are lumped with the inertia of the motor, J, and friction coefficient B.

2. The piston has an effective area A which characterizes how the pressure gradients within the pump, the surface normals of the gear teeth, and the rotational axis of the gears are related.

3. The parameter k_t is the familiar DC motor torque constant.

4. The parameter k_s is the "screw equivalence" of the gear pump. It relates the torque to the force by $\tau = Fk_s$ and the rotation to the displacement by $\theta = x/k_s$.

5. The back flow channel in Fig.11 represents the leakage back through the pump due to the pressure differential across the piston, $p_2 - p_1$. This quantity reflects the fact that at maximum pressure, no net fluid flows through the pump but the rotor is still turning.

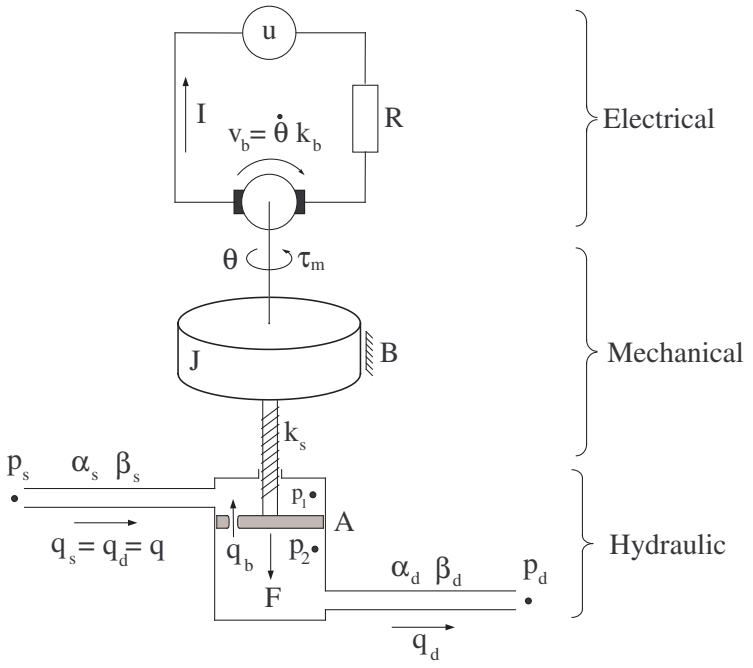

Figure 11: Perpetual power screw model of the gear pump

The electro-mechanical model of the DC motor of the pump is the rotational analog of the VCA considered above.

The angular velocity and acceleration of the motor rotor is related to the applied torques by the familiar 2^{nd} order equation

$$J\ddot{\theta} + B\dot{\theta} = \tau_p + \tau_m \tag{3.19}$$

where J and B represent the rotor moment of inertia, and the bearing friction,

respectively. The torque τ_p is due to the pressure differential across the piston which causes a moment about the fictitious screw due to the screw coefficient k_s. The torque τ_m is the torque generated by the current through the motor windings.

$$\tau_m = Ik_t \tag{3.20}$$

$$\tau_p = Fk_s = A(p_1 - p_2)k_s \tag{3.21}$$

The pressure difference $p_1 - p_2$ may be thought of as the total pressure difference along the pressure gradient which traces a path along gear teeth, starting at the suction port and ending at the discharge port.

The electric circuit for the DC motor of the pump is depicted in Fig.11. Applying Kirchoff's voltage law and solving for I

$$I = -\frac{k_b}{R}\dot{\theta} + \frac{1}{R}u \tag{3.22}$$

By conservation of mass, the volume displaced by the piston (the gear teeth) must be equal to the fluid volume leaving the pump, q, and the fluid that flows back through the teeth, q_b

$$A\dot{x} = Ak_s\dot{\theta} = q_b + q \tag{3.23}$$

Assuming the inertance of the back flow is negligible and that it is related linearly to the pressure differential [13]

$$q_b = \frac{p_2 - p_1}{\alpha'} \tag{3.24}$$

The fluid flow out of and into the pump, q, is related to the discharge and suction pressures by the equations

$$p_s - p_1 = \alpha_s q|q| + \beta_s \dot{q} \tag{3.25a}$$

$$p_2 - p_d = \alpha_d q|q| + \beta_d \dot{q} \tag{3.25b}$$

Defining the parameters $\alpha := \alpha_s + \alpha_d$ and $\beta := \beta_s + \beta_d$ and adding Eq.3.25a to Eq.3.25b

$$(p_s - p_d) + (p_2 - p_1) = \alpha q|q| + \beta \dot{q} \tag{3.26}$$

Eqs.3.19-3.26 may be combined to form

$$\phi_1 \ddot{q} + \phi_2 \dot{q} + \phi_3 q + \phi_4 |q|\dot{q} + \phi_5 |q|q + \phi_6(\dot{p}_d - \dot{p}_s) + \phi_7(p_d - p_s) = u \tag{3.27}$$

If the suction port of the pump is connected to a sufficiently large fluid reservoir, the suction pressure may be assumed constant, which simplifies the equation

$$\phi_1 \ddot{q} + \phi_2 \dot{q} + \phi_3 q + \phi_4 |q|\dot{q} + \phi_5 |q|q + \phi_6 \dot{p}_d + \phi_7(p_d - p_s) = u \tag{3.28}$$

The parameters ϕ_i are

$$\phi_1 = \frac{JR\beta}{k_t A\alpha' k_s} \tag{3.29a}$$

$$\phi_2 = \frac{A^2 k_s^2 R\alpha'\beta + JR\alpha' + BR\beta + 2k_b k_t \beta}{k_t A\alpha' k_s} \tag{3.29b}$$

$$\phi_3 = \frac{BR\alpha' + 2k_b k_t \alpha'}{k_t A\alpha' k_s} \tag{3.29c}$$

$$\phi_4 = \frac{2JR\alpha}{k_t A\alpha' k_s} \tag{3.29d}$$

$$\phi_5 = \frac{A^2 k_s^2 R\alpha'\alpha + 2k_b k_t \alpha + BR\alpha}{k_t A\alpha' k_s} \tag{3.29e}$$

$$\phi_6 = \frac{JR}{k_t A\alpha' k_s} \tag{3.29f}$$

$$\phi_7 = \frac{2k_b k_t + A^2 k_s^2 R\alpha' + BR}{k_t A\alpha' k_s} \tag{3.29g}$$

At steady state Eq.3.28 reduces to

$$\phi_7(p_d - p_s) = u - \phi_3 q_d - \phi_5 q|q| \tag{3.30}$$

Which gives the so-called *characteristic curve*[2] of the gear pump. The Δp versus q curve of Fig.12 is the manufacturer-provided data for the gear pump used for the prototype, the No. 0190 KAVAN GmbH *Geared Electric Pump*, and, as can be seen, follows the quadratic form of Eq.3.30 well.

3.2 System models

As discussed in Section 2, the system operation is divided into Stages I and II. During Stage I, the mitral valve remains open while fluid is pumped from the ventricle into the reservoir. Stage I may be maintained indefinitely as long

[2]Or the pump *head-capacity* curve.

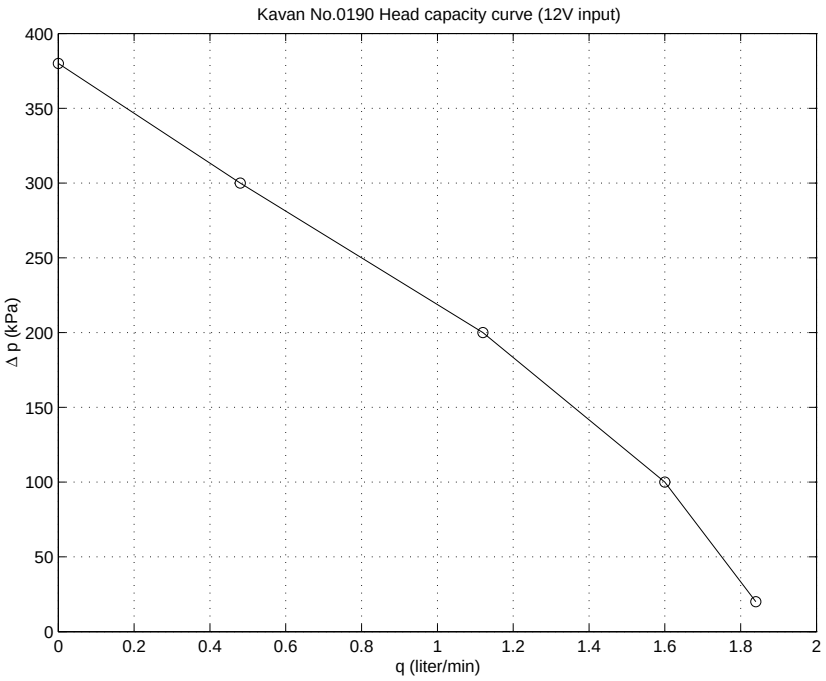

Figure 12: Manufacturer supplied gear pump head capacity curve.

as the ventricular pressure is not brought too low (risking chamber collapse); consequently, due to its simplicity, a Stage I model will not be presented.

While the Stage II model may be viewed as a multiple input single output system (MISO), the tractability of the modeling and control problem is improved greatly if the effects of the two pumps on the ventricular pressure are modeled separately and two separate controllers designed.

3.2.1 Stage II system model (gear pump)

If we assume (rather boldly) that the ventricle behaves like a simple compliant element, and that there is no mitral regurgitation, the Stage II (gear pump) system model appears like that depicted in Fig.13.

Since the intake port of the pump may be considered to be the entire conduit connecting the pump to the fluid reservoir, the suction pressure p_s

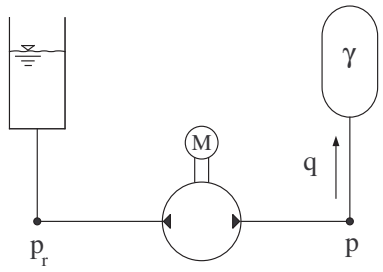

Figure 13: Stage II system model with simplified ventricle (pump details omitted).

equals the reservoir pressure p_r. Likewise, the discharge port may be considered the entire conduit connecting the pump to the ventricle so that the discharge pressure p_d is equal to the ventricular pressure p.

Differentiating Eq.3.7 three times, and substituting the result into Eq.3.28 we obtain the System II (gear pump) model

$$\phi_1\gamma\dddot{p} + \phi_2\gamma\ddot{p} + (\phi_3\gamma + \phi_6)\dot{p} + \phi_4\gamma^2|\dot{p}|\ddot{p} + \phi_5\gamma^2|\dot{p}|\dot{p} + \phi_7(p - p_r) = u \quad (3.31)$$

If we let $\alpha' = \infty$ by assuming the back flow is negligible, ϕ_1, ϕ_4, and ϕ_6 become zero.

Renaming sums and products of parameters to simplify, we have the final form of the Stage II model

$$\varphi_1\ddot{p} + \varphi_2\dot{p} + \varphi_3|\dot{p}|\dot{p} + \varphi_4(p - p_r) = u \quad (3.32)$$

where $\varphi_1 = \phi_2\gamma$, $\varphi_2 = \phi_3\gamma$, $\varphi_3 = \phi_5\gamma^2$, and $\varphi_4 = \phi_7$.

3.2.2 Stage II system model (VCAD pump)

During Stage II (VCAD pump), the gear pump is assumed deactivated, reducing the system to that shown in the top diagram of Fig.14. The quantities α_r and β_r are the combined fluid resistance and inertance of the gear pump and the conduits between the common node and the reservoir. The fluid leaking through the gear pump when it is off, however, is very small relative to the fluid passing from the VCAD pump to the ventricle and may be neglected. The final model is shown at the bottom of Fig.14.

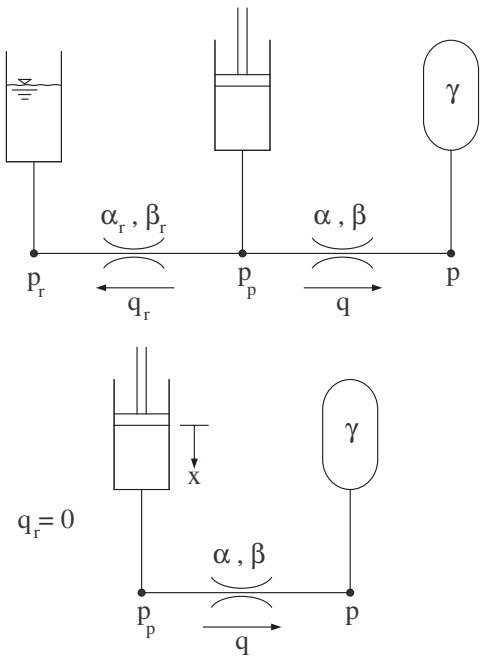

Figure 14: Stage II (VCAD pump) system model. The bottom figure represents the assumption that the flow through the gear pump when it is off may be neglected. Pump details omitted.

Assuming again that the ventricle may be modeled as a simple compliant

element, the governing equations of the Stage II (VCAD pump) system are

$$\dot{p} = \frac{1}{\gamma}q \tag{3.33a}$$

$$\ddot{q} = \frac{A}{\beta\gamma_e}\dot{x} - \frac{1}{\beta\gamma_e}q - \frac{1}{\beta}\dot{p} - \frac{2\alpha}{\beta}|q|\dot{q} \tag{3.33b}$$

$$\ddot{x} = -\left(\frac{c}{m} + \frac{k_b k_f}{mR}\right)\dot{x} - \frac{k}{m}x - \frac{A}{m}p_p + \frac{k_f}{mR}u \tag{3.33c}$$

$$\dot{p}_p = \frac{A}{\gamma_e}\dot{x} - \frac{1}{\gamma_e}q \tag{3.33d}$$

However, if it is assumed that the compliance γ_e of the VCAD pump diaphragm is very small relative to compliance of the ventricle, the state equations may be further simplified

$$\ddot{x} = -\left(\frac{c}{m} + \frac{k_b k_f}{mR}\right)\dot{x} - \frac{k}{m}x - \frac{A}{m}p_p + \frac{k_f}{mR}u \tag{3.34a}$$

$$q = A\dot{x} \tag{3.34b}$$

$$p = \frac{A}{\gamma}x \tag{3.34c}$$

$$p_p = p + \alpha|q|q + \beta\dot{q} = \frac{A}{\gamma}x + \alpha A^2|\dot{x}|\dot{x} + \beta A\ddot{x} \tag{3.34d}$$

Eqs.3.34 may be reduced to the single equation

$$\vartheta_1\ddot{p} + \vartheta_2\dot{p} + \vartheta_3 p + \vartheta_4|\dot{p}|\dot{p} = u \tag{3.35}$$

where the parameters ϑ_i are

$$\vartheta_1 = \frac{m\gamma R + A^2 R\beta\gamma}{k_f A} \tag{3.36a}$$

$$\vartheta_2 = \frac{c\gamma R + k_b k_f \gamma}{k_f A} \tag{3.36b}$$

$$\vartheta_3 = \frac{k\gamma R + A^2 R}{k_f A} \tag{3.36c}$$

$$\vartheta_4 = \frac{A^2 R\alpha\gamma^2}{k_f A} \tag{3.36d}$$

3.2.3 Linear discrete system models

Ultimately, the system controller will be implemented using a microcontroller so it is helpful at this point to derive the discrete linear form of the system models.

The system dynamics are of the form

$$\psi_1\ddot{y} + \psi_2\dot{y} + \psi_3 y + \psi_4|\dot{y}|\dot{y} = u \tag{3.37}$$

This equation, which is identical in form to Eq.3.35, applies to both of the Stage II gear and VCAD pump models; for the gear pump system model $y := p - p_r$, with p_r assumed constant. For the VCAD system model, $y := p$.

Linearizing Eq.3.37 leads to

$$\psi_1\ddot{y} + \psi_2\dot{y} + \psi_3 y = u \tag{3.38}$$

Making the following discrete approximations of the derivatives,

$$\dot{y} \approx \frac{y_{k+1} - y_k}{T} \tag{3.39a}$$

$$\ddot{y} \approx \frac{\dot{y}_{k+1} - \dot{y}_k}{T} = \frac{y_{k+2} - 2y_{k+1} + y_k}{T^2} \tag{3.39b}$$

where y_k implies the value of y at the k^{th} time step, and T is the time step size.

Substituting Eqs.3.39 into Eq.3.38 and collecting terms, we have

$$a_1 y_{k+2} + a_2 y_{k+1} + a_3 y_k = u_k$$

Shifting back two steps

$$a_1 y_k + a_2 y_{k-1} + a_3 y_{k-2} = u_{k-2} \tag{3.40}$$

The parameters a_i are

$$a_1 = \frac{\psi_1}{T^2} \tag{3.41a}$$

$$a_2 = \frac{T\psi_2 - 2\psi_1}{T^2} \tag{3.41b}$$

$$a_3 = \frac{T^2\psi_3 - T\psi_2 + \psi_1}{T^2} \tag{3.41c}$$

It remains then only to determine the parameters a_i before a controller may be designed. First, however, the physical construction of the pump system is specified in more detail.

4 Physical design considerations

The components of the system should be chosen such that achievable pressure and flow rates meet those of the animal heart under study. Table 1 contains a sample of biometric data taken from the literature.

Table 1: Sampling of physical data taken from the literature.

Specimen	canine [16, 17]	equine [18, 19]	porcine [20, 21]
stroke (cm^3)	39.7	900	39
rate ($\frac{1}{min}$)	199	275	103
$\gamma(\frac{m^3}{Pa})$			7E-9 to 50 E-9
$p_{sys}(Pa)$	16E+3 to 28E+3	27E+3	16E+3
$p_{dia}(Pa)$	1.33E+3		

A very conservative way to size the gear pump for the design is to base the selection on whether the point $\left(\gamma\frac{p_{sys}-p_{dia}}{T_{sys}},\ \ p_{sys}-p_{dia}\right)$ lies under the head capacity curve of the pump; Fig.15 illustrates this point. The abscissa is the ratio of the excess volume which will raise the ventricle to p_{sys}, to the period of the systole, T_{sys}. The ordinate is the total increase in pressure during the systole.

4.1 Fluid reservoir

The fluid reservoir must be sufficiently large to maintain near-constant pressure. If it is assumed that the system could expand enough to remove a volume ΔV of fluid, and that it is desired that the reservoir pressure change by less than $\pm\Delta p$, the diameter D of a cylindrical reservoir is constrained by

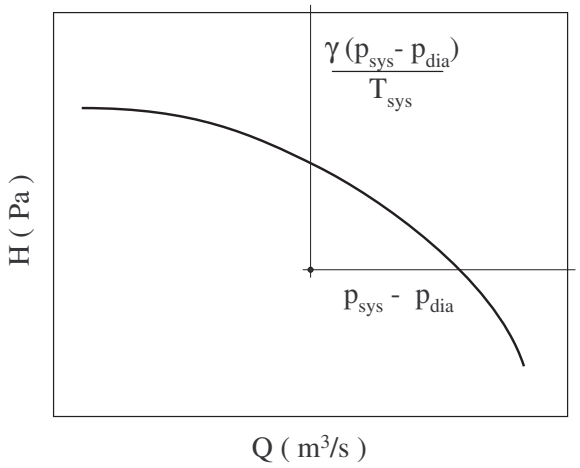

Figure 15: Choosing a suitable gear pump. The curve represents a typical pump head capacity curve. If the point is under the curve, the pump has more than enough capacity to drive the system at a frequency comparable to a living specimen.

the relation

$$D > \sqrt{\frac{4\rho g}{\pi}\frac{\Delta V}{\Delta p}} \tag{4.1}$$

For example, assuming that the whole system could expand enough to remove 1 liter of water from the reservoir (which is approximately the stroke of an equine heart, for example), and it is desired to keep the reservoir pressure at $\pm 10\%$ of the nominal p_r (the average porcine/human diastolic pressure is similar to the canine at around $p_{dia} = 1.3\ kPa$), the diameter must then be at least 27.45 cm.

4.2 VCAD pump design

Exploded and assembled views of a prototype VCAD pump assembly are shown in Figs.16 and 17.

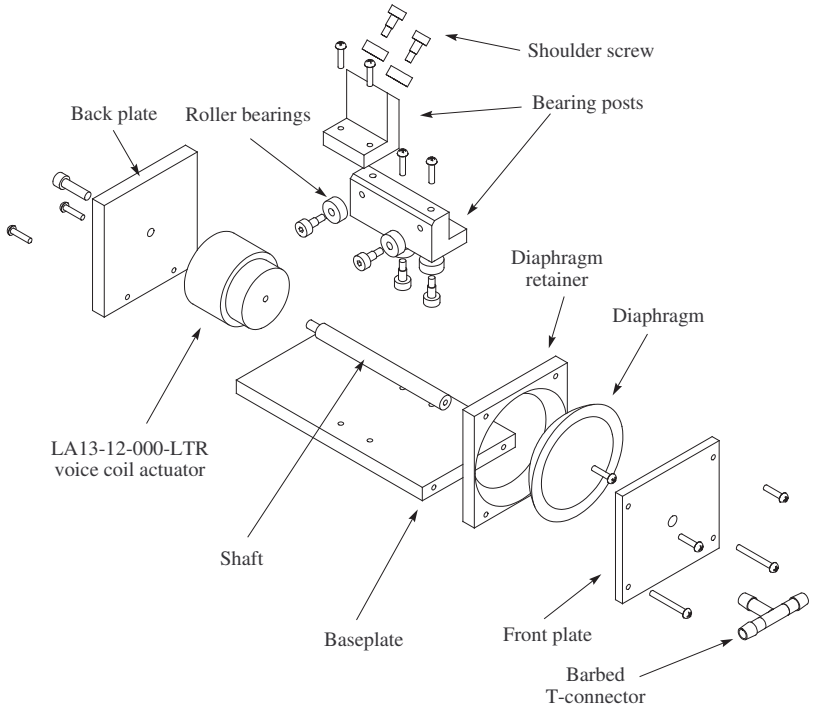

Figure 16: The voice coil actuated diaphragm pump. Exploded view.

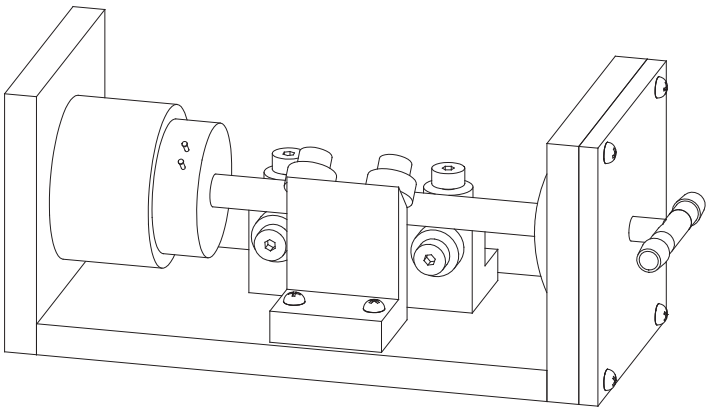

Figure 17: VCAD assembled view.

The assembly consists of rubber diaphragm whose flange is is clamped between two aluminum plates. The main frame of the pump consists of aluminum base- and back-plates and two bearing posts. Mounted to the bearing posts are six roller bearing arranged in a triangular configuration to constrain motion of the shaft in the axial direction relative to the VCA.

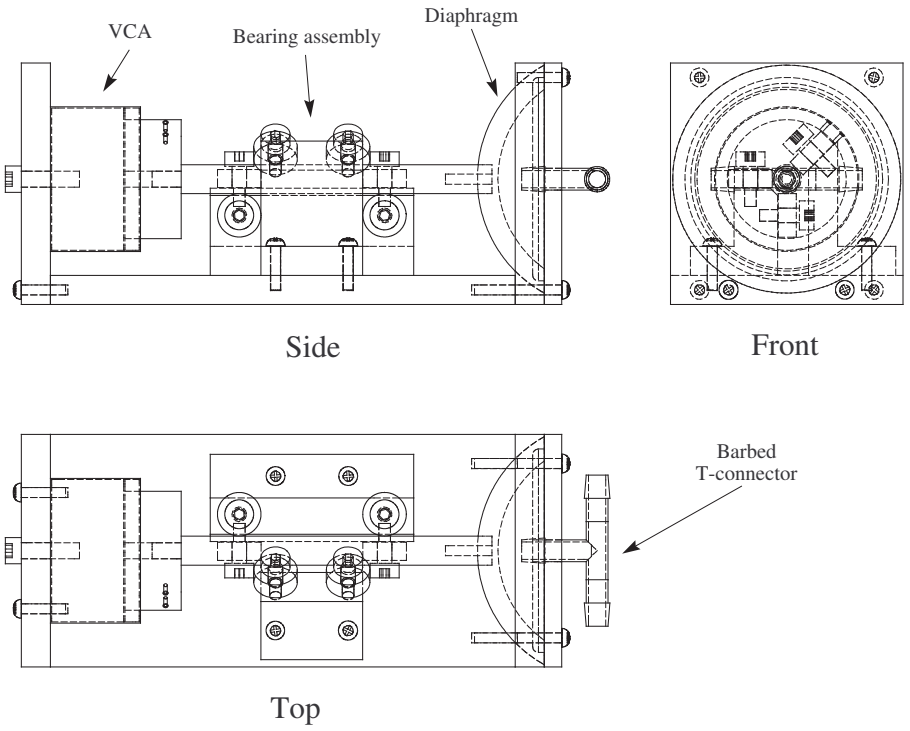

Figure 18: VCAD three-view

Fig.19 contains a photograph of the prototype VCAD pump connected to a $12V$ gear pump. The VCA used for the prototype is a LA13-12-000-LTR linear voice coil actuator provided by BEI KIMCO [22].

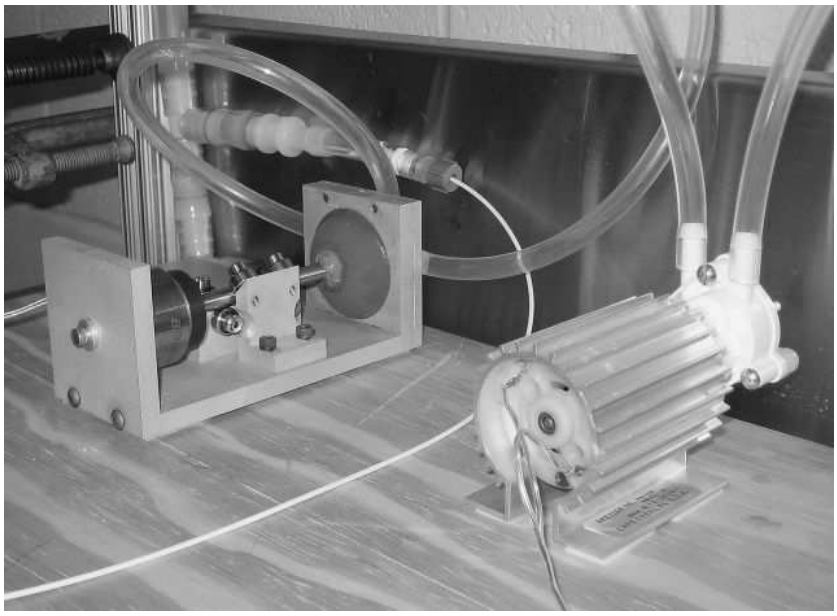

Figure 19: A photograph of the prototype VCAD pump (shown with a 12V gear pump).

5 Electronic controller implementation

The circuit for the pump controller consists of three main circuit blocks:

1. A microcontroller circuit based on the Microchip 18F4520 is used to acquire pressure measurements and control the pumps.

2. A sensor/amplifier circuit converts fluid pressure to a conditioned voltage signal for acquisition.

3. An H-bridge and associated logic circuitry power the pumps.

5.1 Microcontroller circuit

The microcontroller chosen for this design needs to have a minimum of two Pulse Width Modulation (PWM) outputs in order control the average volt-

age applied to the H-bridges (which is a cost-effective and efficient alternative to continuous or analog voltage control), and an Analog to Digital Converter to take digital readings from the sensor amplifier. The 8-bit 18F4520 from Microchip [23] meets these requirements and has the added benefits of requiring little external circuitry, is optimized for C code programming, has an 8x8 hardware multiplier, and is available in a DIP package for easy prototyping. Fig.20 contains the pin-out diagram of the 18F4520.

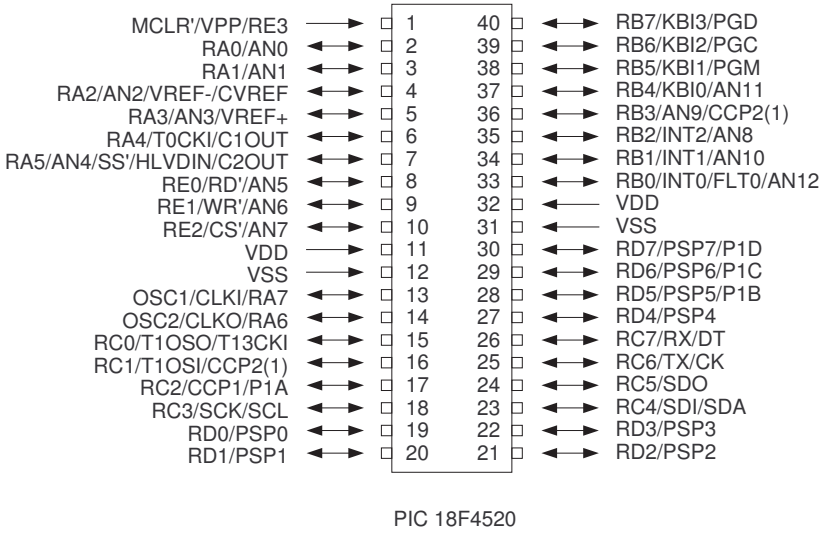

Figure 20: Pin-out diagram of the 18F4520

The core microcontroller circuit is shown in Fig.21. Omitted from the schematic are any human interface components other than the reset switch s_1.

5.2 Sensor circuit

The pressure sensor used for the prototype is the Motorola MPX2050 50 kPa Temperature Calibrated Pressure Sensor [24]. The sensor has two pressure

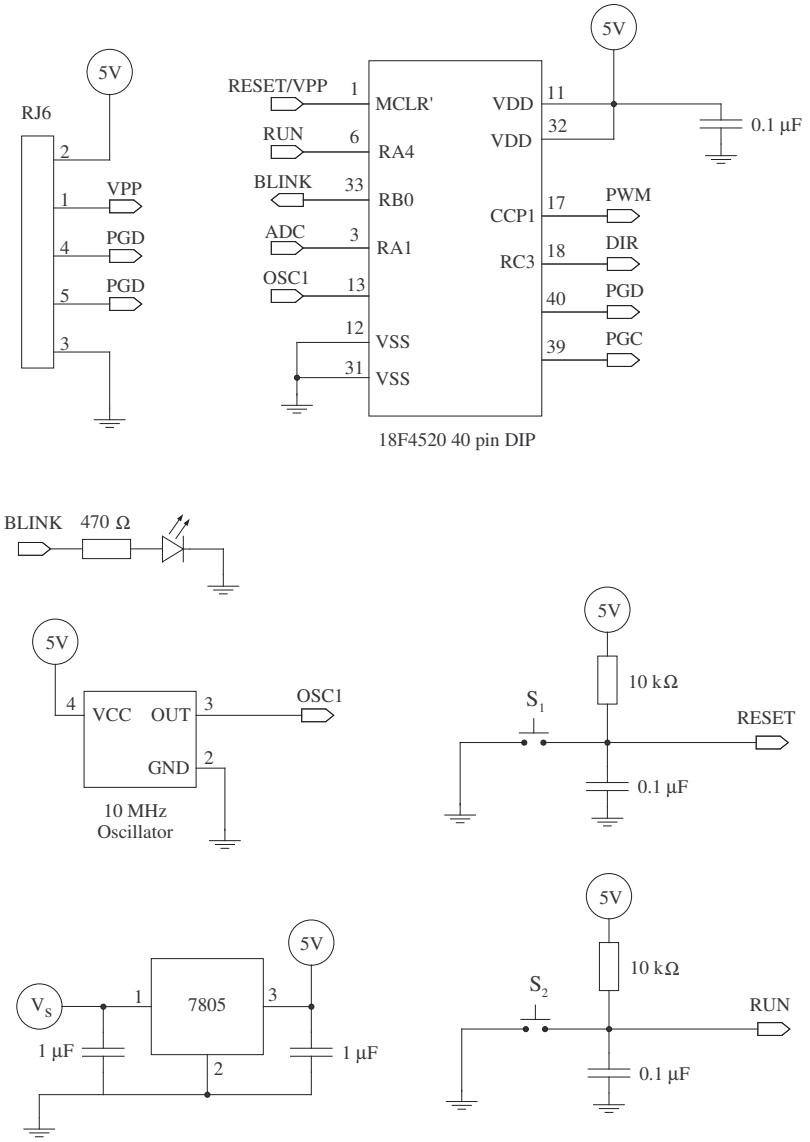

Figure 21: The core microcontroller circuit (top). V_s is the power supply input. A $12V$, $4A$ power supply was used for the prototype. The assembly consisting of the RJ6 connector is to allow in-circuit serial programming of the microcontroller using an ICD2 programmer [1]. Switch S_1 resets the microcontroller, while S_2 is a "dead man's switch" that must be held down for the system to operate.

input ports and two accompanying electrical outputs. The voltage difference across the outputs varies linearly with the pressure differential across the input ports.

The linear "sensitivity" (input-output) relationship g is approximately

$$g := \frac{v_{out}}{p_{in}} = 8 \times 10^{-4} \frac{V}{kPa}$$

Assuming that at $p_{in} = p_{sys} = 16kPa$ and that we require $v_{out} = 4.5Volt$ (maximum), an amplifier gain $G = \frac{4.5Volt}{(16kPa)(g)} \approx 350$ is required.

The amplifier design used is based on the "High input Z adjustable gaind [*sic*] DC instrumentation amplifier" described in [25]. The gain for the instrumentation amplifier is given by

$$G = \left(1 + \frac{2R}{R_g}\right) \tag{5.1}$$

Assuming $R = 100k\Omega$, R_g should be approximately 570Ω. A $1k\Omega$ trimmer resistor was used for the prototype. The complete circuit is shown in Fig.22.

In practice, the sensor output voltage v is related to the pressure input p according to

$$p = p_s v_{out} + p_0 \tag{5.2}$$

The slope p_s and offset p_0 must be determined experimentally for each sensor/amplifier combination.

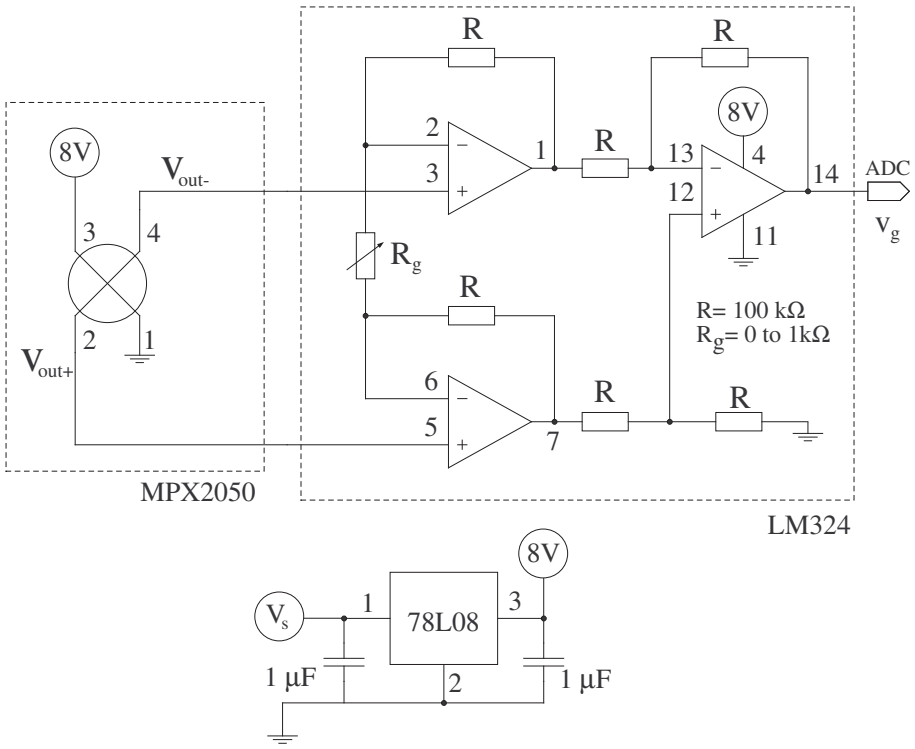

Figure 22: Instrumentation amplifier with sensor

5.3 H-bridge circuit

The H-bridge circuit used for the prototype to drive either the gear pump or the VCA is shown in Fig.23. H-bridges allow the use of single-sided power supplies by toggling the polarity of the voltage applied to the motor, and are able to handle higher currents than the outputs of the microcontroller's PWM module. The main circuit (top of figure) is based on the Infineon TLE 5205-2 H-bridge [26]. The truth table for the H-bridge is given in Table 2.

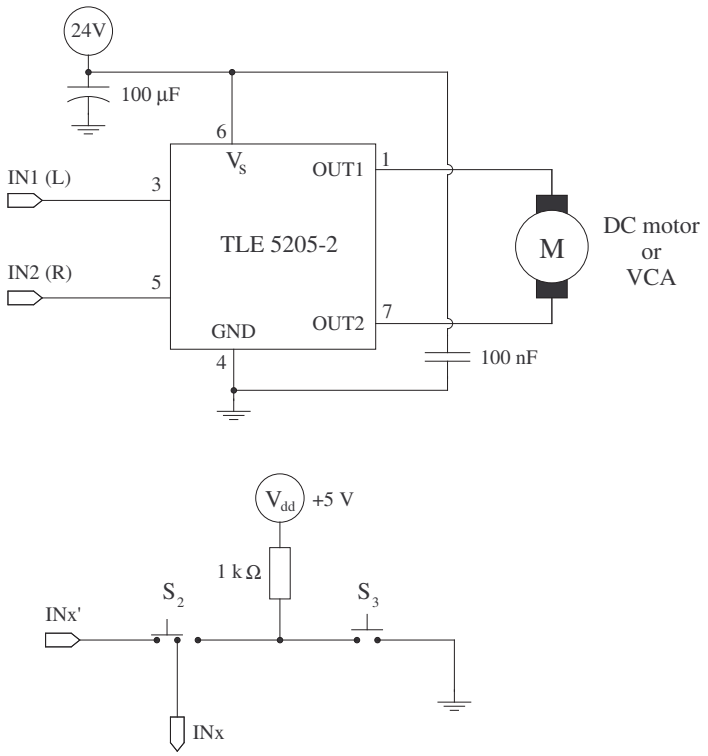

Figure 23: H-bridge VCAD/gear pump driver. The bottom circuit allows manual control of the motors. Switch s_2 determines whether the microcontroller or switch s_3 controls the motor. There are two manual control circuits per motor, one to control direction and one to switch the motor on or off (the x denotes either 1 or 2).

Looking at the H-bridge truth table, there appears no obvious way to achieve forward/backward control of a motor using a single PWM signal. It is desired to control each actuator using two microcontroller outputs: a direction output D which controls the polarity of the H-bridge output, and a pulse output P which serves as the PWM signal. Table 3 contains the truth table relating the *desired* input to the *required* output.

Table 2: Truth table for the TLE5205-2 H-bridge. The OCD state (open circuit detection) is an unused diagnostic function, but allows the motor to turn freely.

$IN1(L)$	$IN2(R)$	$OUT1$	$OUT2$	$function$
0	0	1	0	forward
0	1	0	1	reverse
1	0	0	0	brake
1	1	z	z	OCD

Table 3: Truth table relating the desired input combination to the required output combination. P is the PWM signal, and D the direction signal. L and R are the H-bridge inputs $IN1$ and $IN2$, respectively.

P	D	L	R
0	0	1	1
0	1	1	1
1	0	0	1
1	1	0	0

When P is low, the motor needs to be off but not braked, so both L and R must be high to allow the motor to rotate freely.

To find the equivalent logic gate structure, sum-of-products equations [27]

may to be written for each output. For output L

$$\overline{P}\ \overline{D} + \overline{P}D = L$$

Factoring out $\overline{P}$ and using the identity $\overline{A} + A = 1$

$$\begin{aligned} \overline{P}(\overline{D} + D) &= L \\ \overline{P} &= L \end{aligned} \tag{5.3}$$

For output R,

$$\begin{aligned} \overline{P}\ \overline{D} + \overline{P}D + P\overline{D} &= R \\ \overline{P} + P\overline{D} &= R \end{aligned}$$

Using the identity $A + \overline{A}B = A + B$

$$\overline{P} + \overline{D} = R \tag{5.4}$$

Eqs.5.3 and 5.4 expressed using only NOR gates is shown in Fig.24. This circuit, which may be implemented using a single 74HCT02 chip [28], is the "glue" logic between the microcontroller and H-bridge. One circuit is required for both the gear pump and VCAD pump.

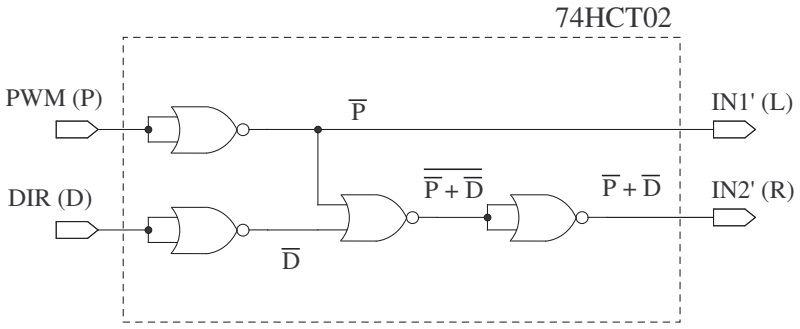

Figure 24: A circuit to convert a DIR/PWM signal pair to that suitable for use by the TLE5205 Hbridge; it is the truth table of Tab.3 expressed using only NOR gates. The resulting circuit is implemented using a single 74HCT02 package.

6 Controller design

Two conventional controllers, a discrete PD and PID are now derived.

6.1 The discrete PID controller

The continuous time PID controller is

$$u = u_P + u_I + u_D \tag{6.1}$$

$$u_P := K_P e \tag{6.2}$$

$$u_I := K_I \int_0^t e(\tau) d\tau = K_I E \tag{6.3}$$

$$u_D := K_D \dot{e} \tag{6.4}$$

Expressed recursively, the integral of the error, E, up to time instant k is approximated as

$$E(k) = E(k-1) + \frac{T}{2}\left(e(k) + e(k-1)\right) \tag{6.5}$$

where $E(k)$ is the integral of the error up to time $t = kT$, and T is the sampling period.

Multiplying through by the integral control gain K_I, the discrete approximation of the integral control input at time k, $u_I(k)$ is

$$u_I(k) = K_I E(k) = u_I(k-1) + \frac{K_I T}{2}\left(e(k) + e(k-1)\right) \tag{6.6}$$

Defining the time-shift operator z as $z^n x(k) := x(k+n)$, the input may be expressed alternatively as

$$u_I(k) = \frac{K_I T}{2}\frac{1+z^{-1}}{1-z^{-1}}e(k) \tag{6.7}$$

The discrete approximation $u_D(k)$ of the derivative control input u_D is the difference quotient

$$u_D(k) = K_D\frac{e(k) - e(k-1)}{T} \tag{6.8}$$

Using time-shift notation,

$$u_D(k) = \frac{K_D}{T}\left(1 - z^{-1}\right)e(k) \tag{6.9}$$

Finally, the proportional input is simply

$$u_P(k) = K_P e(k) \tag{6.10}$$

The complete PID input using time-shift notation is then

$$u(k) = K_P e(k) + \frac{K_D}{T}\left(1 - z^{-1}\right) e(k) + \frac{K_I T}{2}\frac{1 + z^{-1}}{1 - z^{-1}} e(k) \tag{6.11}$$

To express the control rule in discrete time form, we first multiply through by[3] $(1 - z^{-1})$

$$\begin{aligned}
(1 - z^{-1})u_k &= K_P(1 - z^{-1})e_k + \frac{K_D}{T}\left(z^{-2} - 2z^{-1} + 1\right) e_k && \text{(6.12a)} \\
&\quad + \frac{K_I T}{2}(1 + z^{-1})e_k \\
u_k - u_{k-1} &= K_P(e_k - e_{k-1}) + \frac{K_D}{T}(e_{k-2} - 2e_{k-1} + e_k) && \text{(6.12b)} \\
&\quad + \frac{K_I T}{2}(e_k + e_{k-1})
\end{aligned}$$

Collecting terms, the discrete time PID controller is expressed finally as[4]

$$\begin{aligned}
u_k &= u_{k-1} + c_1 e_k + c_2 e_{k-1} + c_3 e_{k-2} && \text{(6.13a)} \\
c_1 &:= K_P + \frac{K_D}{T} + \frac{K_I T}{2} && \text{(6.13b)} \\
c_2 &:= \frac{K_I T}{2} - \frac{2K_D}{T} - K_P && \text{(6.13c)} \\
c_3 &:= \frac{K_D}{T} && \text{(6.13d)}
\end{aligned}$$

Fig.25 contains a general flow chart for the digital PID control loop.

6.1.1 Controller gains

As long as T is much shorter than the smallest time constant of the system [13], the control gains may be determined using methods from continuous

[3]The notations $x(k)$ and x_k are equivalent and will be used interchangeably.
[4]This derivation is inspired by [13] and [29].

control theory. The optimal gains for a "uniform damping/stiffening" PID controller are

$$K_P = 3\lambda^2\psi_1 + (\sigma^2 - 1)\psi_3 \tag{6.14a}$$

$$K_D = 3\lambda\psi_1 - \psi_2 \tag{6.14b}$$

$$K_I = \lambda\sigma^2\psi_3 \tag{6.14c}$$

The terms λ and σ are the designer determined closed-loop decay rate and stiffening factor, respectively.

Inverting Eqs.3.41 to find ψ_i, substituting into Eq.6.14, and finally substituting the result into Eq.6.13, we have the coefficients of the discrete PID controller in terms of the system parameters a_i, the sampling period T, and the design specifications λ and σ,

$$\begin{aligned} c_1 = {} & \left(3\lambda^2T^2 + \sigma^2 + {}^1\!/_2\lambda\sigma^2T + 3T\lambda - 3\right) a_1 \\ & + \left(\sigma^2 + {}^1\!/_2\lambda\sigma^2T - 2\right) a_2 \\ & + \left({}^1\!/_2\lambda\sigma^2T + \sigma^2 - 1\right) a_3 \end{aligned} \tag{6.15a}$$

$$\begin{aligned} c_2 = {} & \left({}^1\!/_2\lambda\sigma^2T - 6T\lambda - \sigma^2 - 3\lambda^2T^2 + 5\right) a_1 \\ & + \left({}^1\!/_2\lambda\sigma^2T - \sigma^2 + 3\right) a_2 \\ & + \left({}^1\!/_2\lambda\sigma^2T - \sigma^2 + 1\right) a_3 \end{aligned} \tag{6.15b}$$

$$c_3 = (3T\lambda - 2)\, a_1 - a_2 \tag{6.15c}$$

6.2 Discrete PD controller

The continuous proportional-derivative controller is

$$u_{pd} = -K_p e - K_v \dot{e} \tag{6.16}$$

which may be approximated discretely as

$$u_k = b_1 e_k + b_2 e_{k-1} \tag{6.17}$$

$$b_1 := K_p + \frac{K_v}{T} \tag{6.18}$$

$$b_2 := -\frac{K_v}{T} \tag{6.19}$$

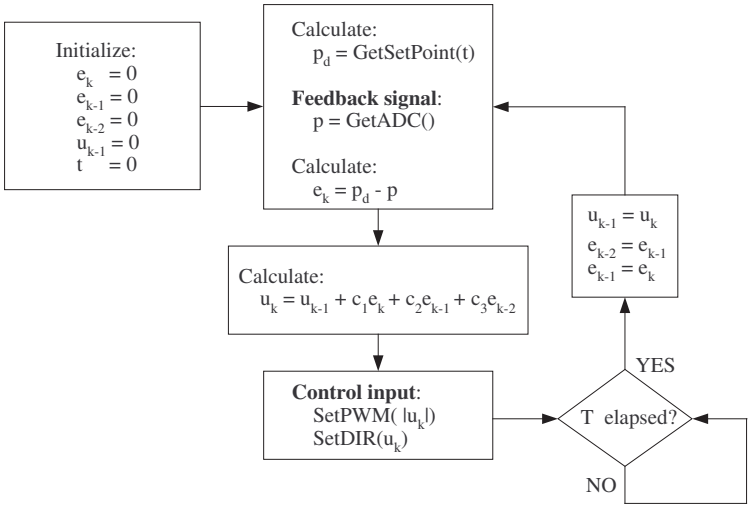

Figure 25: The basic discrete PID control flow chart. The function *GetSetPoint(t)* returns the desired pressure at time t. *GetADC()* returns the current analog-to-digital reading. *SetPWM($|u_t|$)* sets the pulse width module duty cycle to the absolute value of the calculated controller input. *SetDIR(u_t)* sets the H-bridge polarity according to the sign of the control input (negative is set to 0, positive to 1). The sampling period is T.

7 Experimental results

To validate the system, two sets of experiments were performed. The first experiment tested the 18F4520 digital controller with a solitary gear pump. The second experiment utilized a controller based on the xPC Target rapid prototyping system along with Simulink to validate the hybrid pumping system.

The experimental setup consisted of the hybrid pump system connected to a large fluid reservoir and a $\gamma = 12 \times 10^{-9} \ \frac{m^3}{Pa}$ compliance vessel which served as the explanted "ventricle".

A triangular velocity trajectory was chosen as the tracking reference. The trajectory consists of four segments, T_{sys}, T_{dia}, T_h, and T_l which are the period of systole, diastole, peak pressure, and rest period, respectively. A schematic of the trajectory is shown in Fig.26.

7.1 Validation of the 18F4520-based controller (gear pump only)

To determine the system and controller parameters, a step input was applied to the system. The response, along with discrete and continuous simulation responses are shown in Fig.28.

Fig.29 contains the results of the PD controller over four cycles with $T_{sys} = 6.5s$, $T_{dia} = 3.4s$ and $T_h = T_l = 0$. As can be seen, the overall tracking performance is reasonable with the exception of the "chattering" that occurs as the gear pump switches direction as the actual pressure path crosses the desired trajectory.

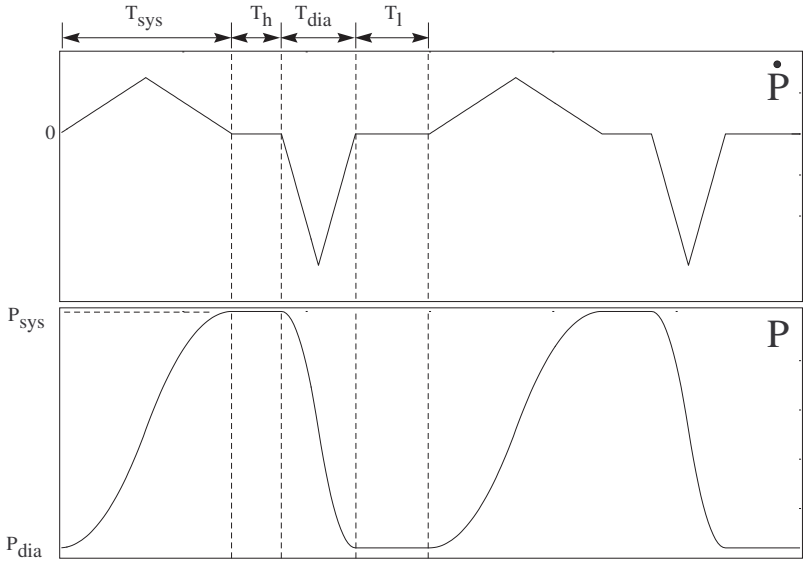

Figure 26: The triangle pressure velocity trajectory (top) with actual pressure (bottom). Two cycles of the velocity $\dot{p}$ and pressure p, are shown. The velocity is the time-rate of change of the pressure; the actual pressure path is therefore the integral of the velocity trajectory.

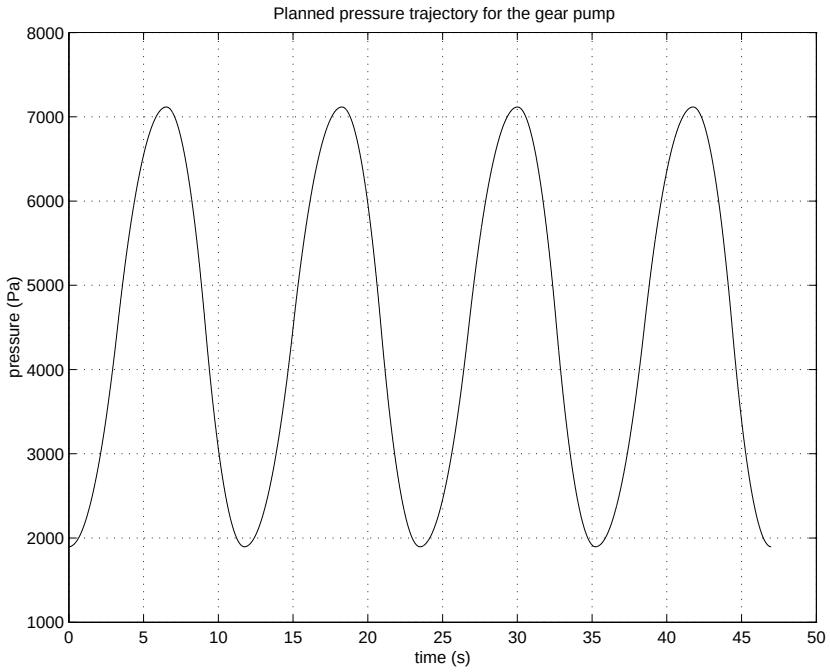

Figure 27: Desired path used validate the 18F4520 controller.

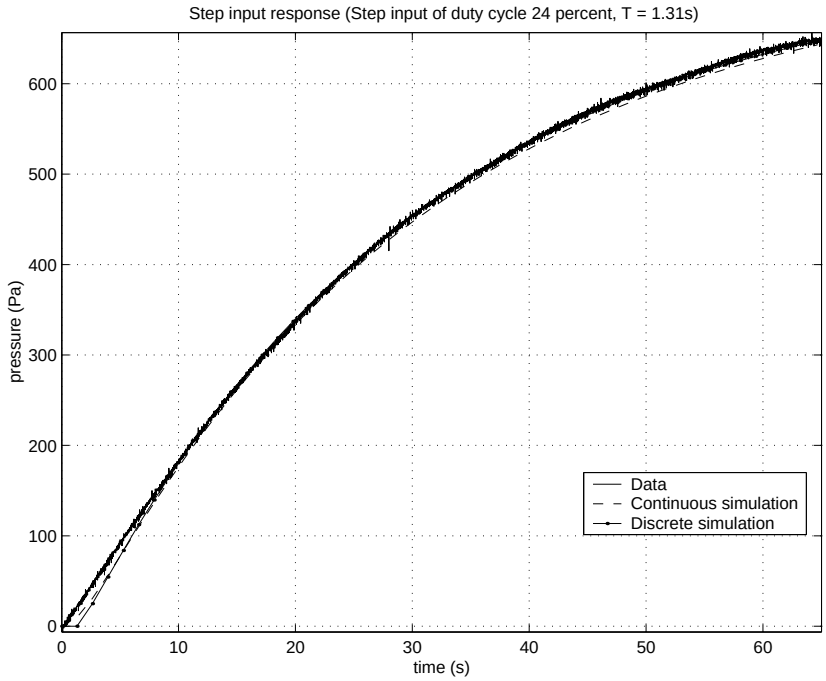

Figure 28: The step input response of the microcontroller system using the KAVAN gear pump.

Regardless of the gains b_i used, the chattering problem is unavoidable due to stiction. As the actual pressure intersects the desired trajectory, the pump must reverse itself causing it to be momentarily stationary, and, consequently, a smooth control response is not possible.

The system performance is improved considerably by using the PID controller.

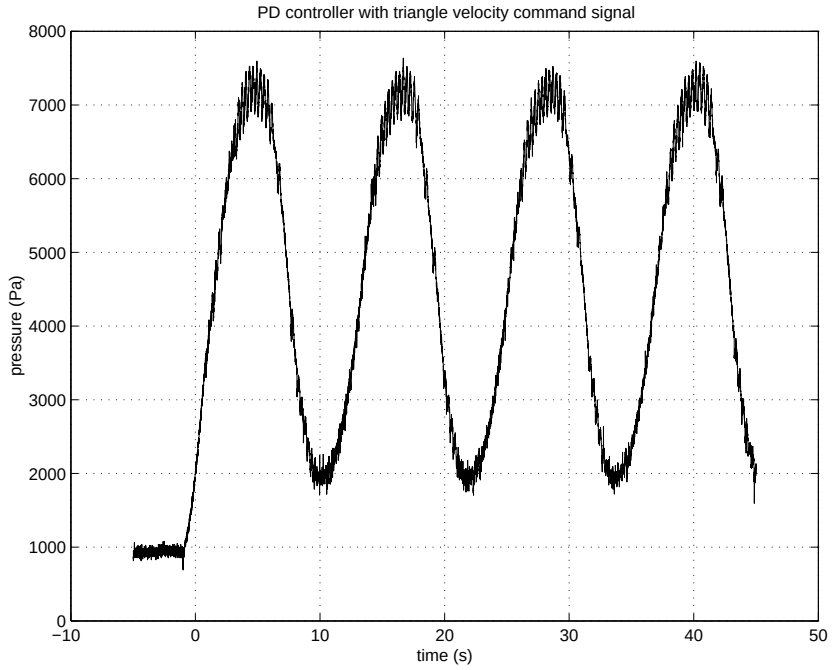

Figure 29: PD Controller performance with a triangle velocity command signal. The target P_{sys} is $7.1kPa$. The target P_{dia} is $1.9kPa$.

Fig.31 contains a plot of the system response data using the PID controller. As can be seen, the chattering problem is noticeably reduced.

The integral term of the PID controller has the effect of reducing the continuous tracking error which thereby reduces the possibility that, as the command trajectory is continuously increasing or decreasing, the pump will need to reverse itself and thereby induce oscillations.

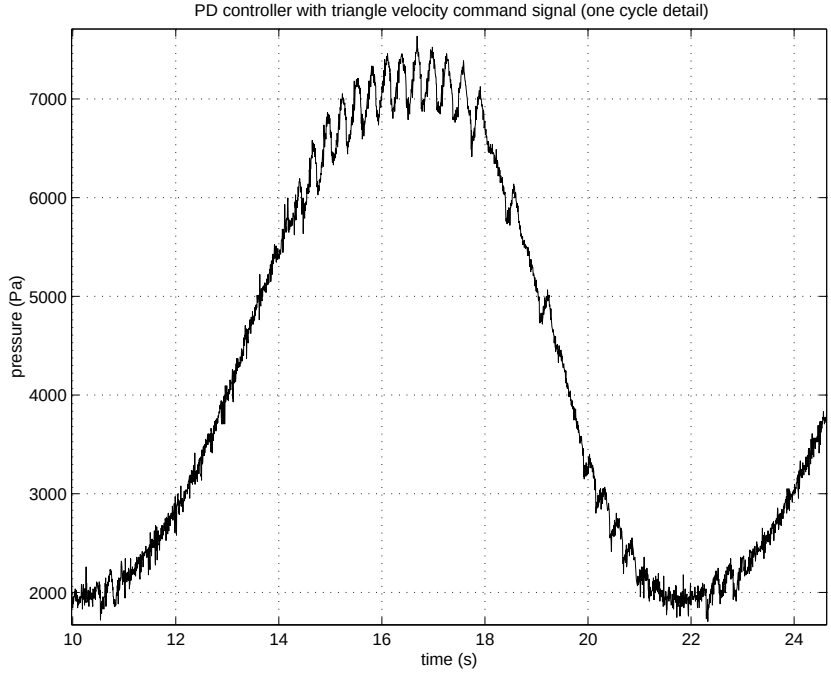

Figure 30: Single cycle detail of Fig.29.

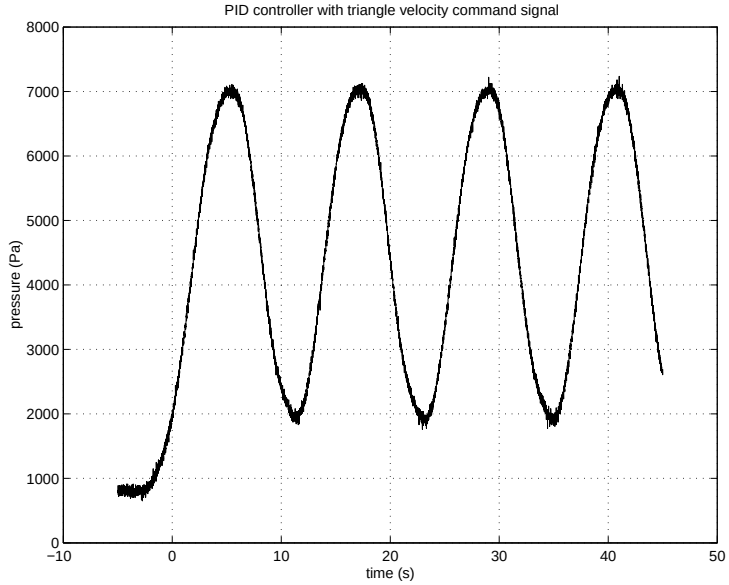

Figure 31: PID Controller performance with a triangle velocity command signal. The target P_{sys} is $7.1kPa$. The target P_{dia} is $1.9kPa$.

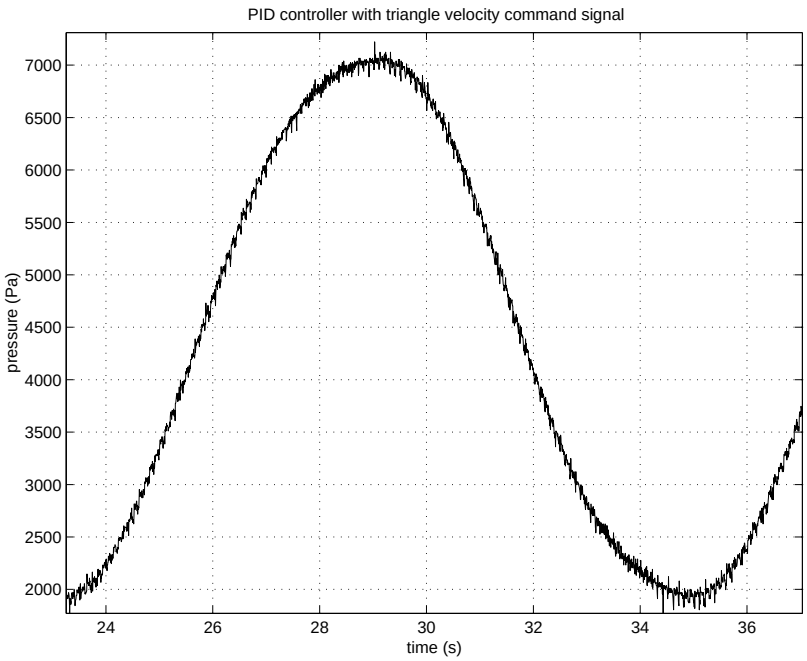

Figure 32: Single cycle detail of Fig.32.

If T_h is set to some nonzero value, say, $5.2s$, the PID controller has difficulty maintaining systolic pressure due to leakage through the gear pump. Fig.34 shows the pressure drop during T_h.

If the gains are stiffened to force the controller to compensate for the back flow, considerable chatter is induced. See Fig.35.

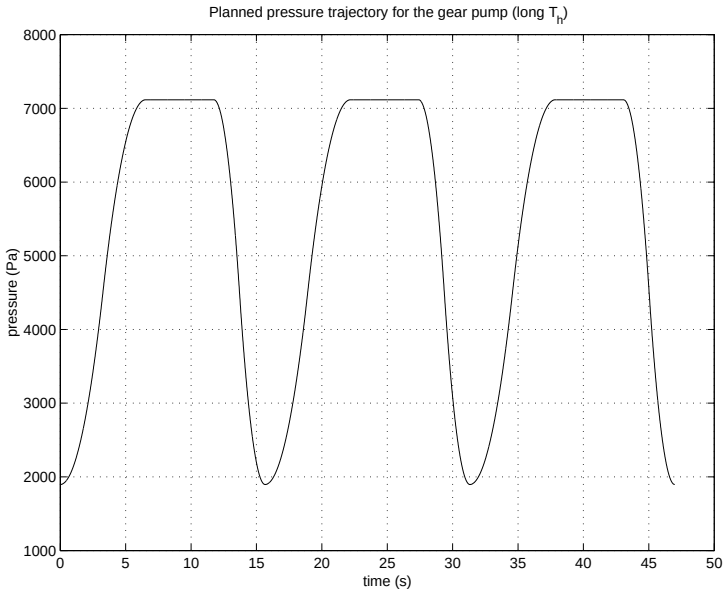

Figure 33: Desired path with $T_h = 5.2s$.

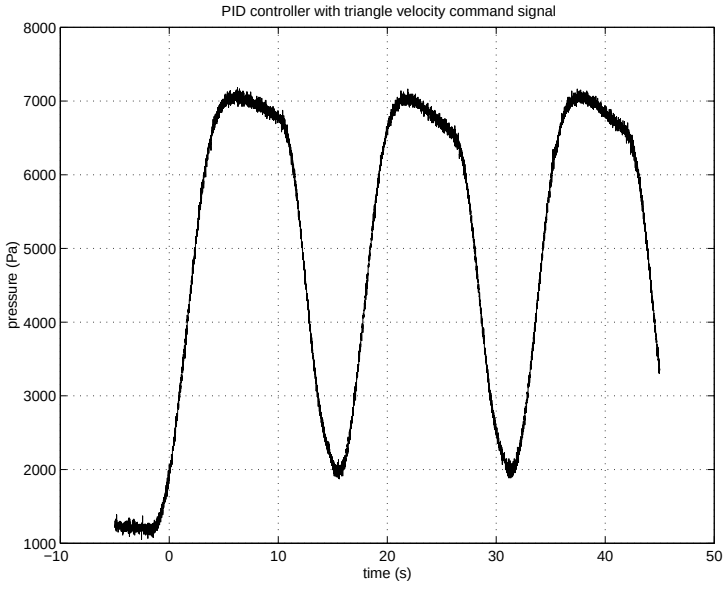

Figure 34: $T_h = 5.2s$. The gear pump cannot maintain systolic pressure indefinitely with the same gains. The pressure drops due to back flow through the gear pump. $\sigma = 4$, $\alpha = 0.1$

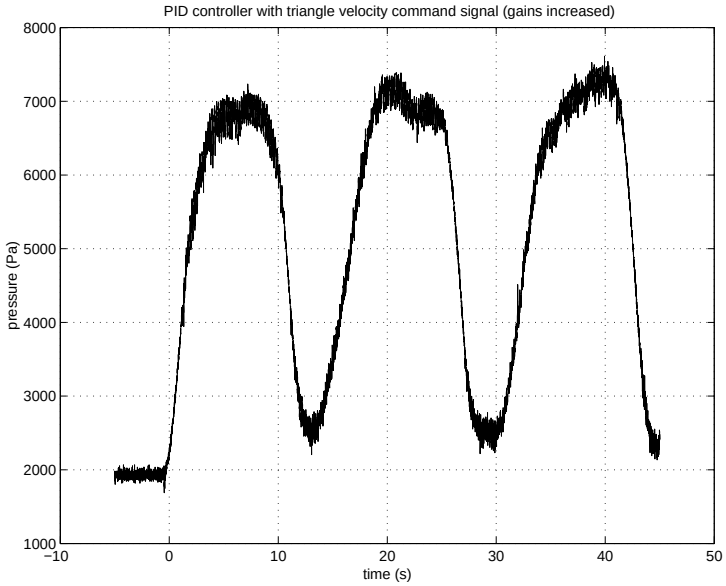

Figure 35: $T_h = 5.2s$. The PID gains are increased and the gear pump induces severe oscillations attempting to maintain P_{sys}. $\sigma = 40$, $\alpha = 0.99$

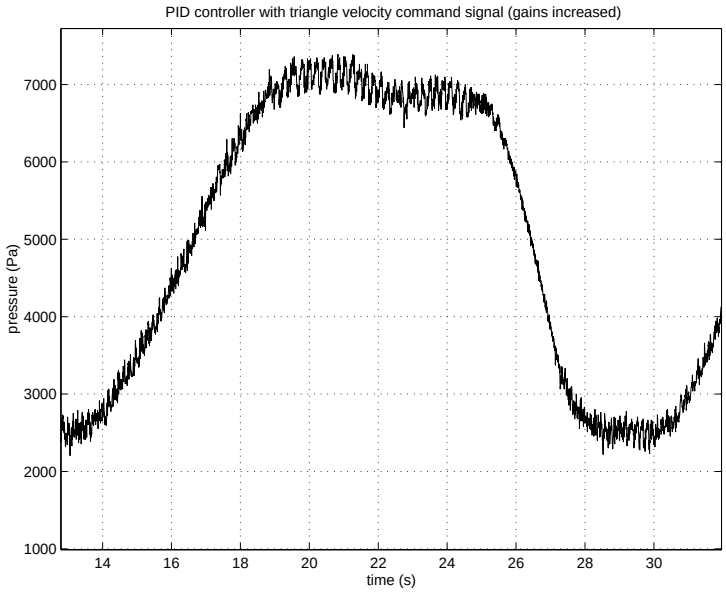

Figure 36: Detail of Fig.35.

7.2 Hybrid pump system performance

Fig.37 superimposes the Bode magnitude plots of the gear and VCAD pumps. The data for the gear pump was generated from the 2^{nd} order transfer function which in turn was found from the step input response. As can be seen, the gear pump gain decreases quite rapidly, with a bandwidth that extends to about 4 rad/s. The VCAD pump performs well within a band between approximately 5 to 100 rad/s.

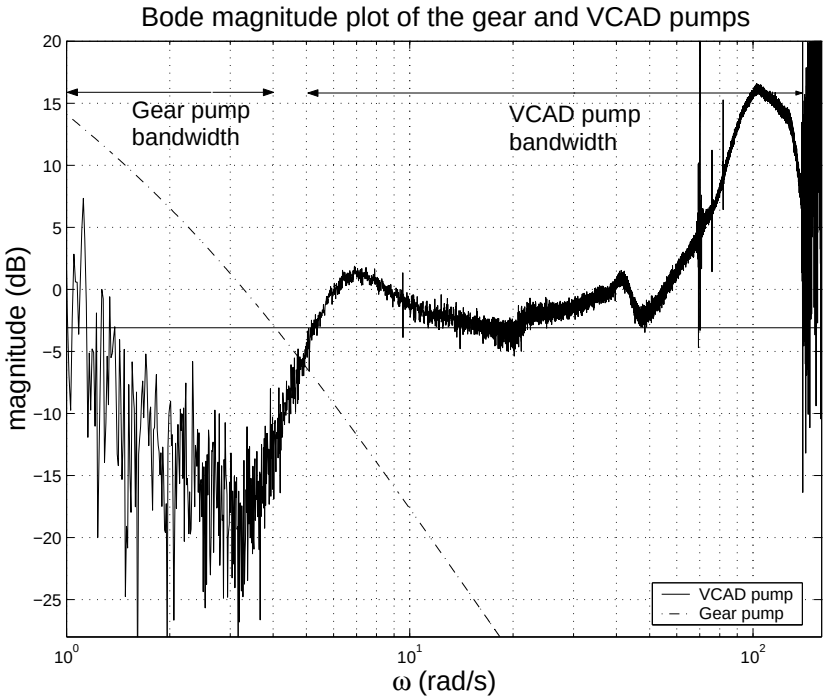

Figure 37: Bode magnitude plots of the gear and VCAD pumps.

Fig.38 superimposes the hybrid system ventricular pressure over the pressure of the gear pump working alone. As can be seen, the high frequency actuation authority exhibited by the VCAD pump in Fig.37 allows the hybrid system to reduce high frequency oscillations due to unmodeled system

dynamics.

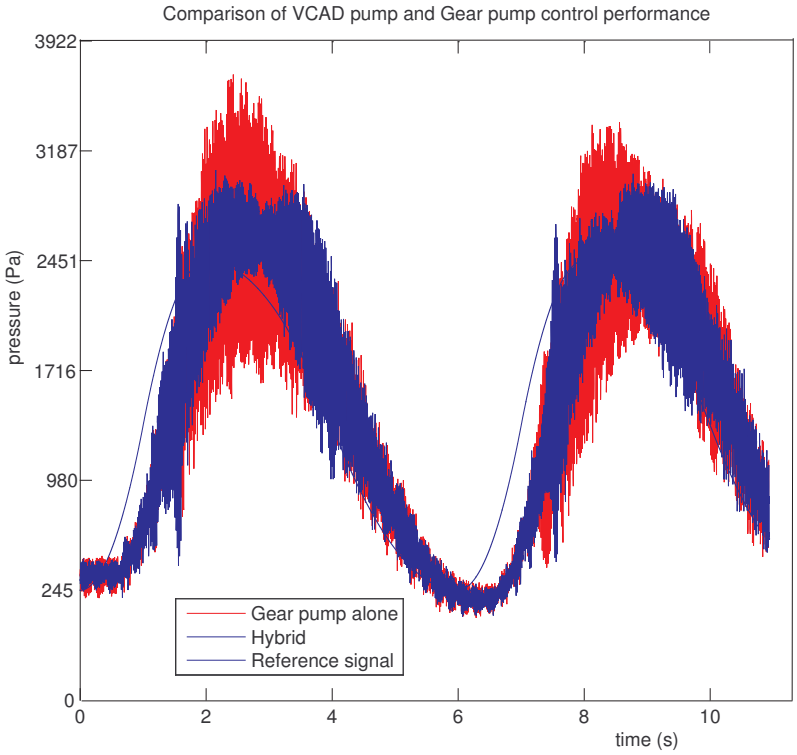

Figure 38: Plot of the hybrid pump system output over two cardiac cycles. The ability of the VCAD pump to control high frequency oscillations may be seen.

8 Conclusion

A new hybrid pump system architecture for the dynamic pressurization of explanted mammalian hearts has been proposed. The system consists of two complementary pumps: a high-bandwidth low-flow voice coil actuated diaphragm (VCAD) pump and a low-bandwidth high-flow gear pump. Mathematical models describing the system dynamics have been developed leading to discrete linear equations which are used in the development of a digital system controller.

A prototype VCAD pump based on the BEI KIMCO LA13-12-000-LTR voice coil actuator along with a simple yet effective bearing system has been designed and built. To control the VCAD and gear pumps, an electronic circuit based on the 18F4520 microcontroller, MPX2050 pressure sensor, and TLE5205-2 H-bridge has also been designed and built. While the 18F4520 proved adequate to control the gear pump, the hybrid VCAD/gear pump system required the use of a more advanced computer controller (the xPC Target system was used). A digital signal controller/processor such as the Microchip dsPIC30F2010, which is designed specifically for motor control applications, appears to be a good platform for further development.

The feasibility of using gear pumps for low frequency pressure tracking in heart pressurization applications has been demonstrated. The low cost and high performance of gear pumps make them attractive alternatives to other types of positive displacement pumps. The bandwidth of the gear pump is indeed limited, however, which demonstrates the need for the hybrid architecture.

The VCA available for the prototype required the use of a low-volume diaphragm resulting in a VCAD pump with very little actuation authority in the middle to low frequency range (the hybrid system exhibits band rejection between 4 and 5 rad/s). This limitation frustrated attempts to demonstrate the ability of the hybrid system to track midrange frequency reference signals. However, the experimentally determined frequency response function of the hybrid pump system validates the hybrid system concept by showing that the gear and VCAD pumps do indeed have complimentary bandwidths. Finally, the high frequency actuation authority of the VCAD pump clearly enabled the hybrid system to control high frequency oscillations due to unmodeled dynamics.

-Fin-

References

[1] Microchip Technology, Inc. *MPLAB ICD 2 In-Circuit Debugger User's Guide (DS51331B)*, 2005.

[2] Mike Rayner and Sophie Petersen. European cardiovascular disease. *British Heart Foundation Health Promotion Research Group,Department of Public Health, University of Oxford, Institute of Health Sciences*, 2000.

[3] Richard Cooper and Jeffrey Cutler et. al. Cardiovascular diseases in the united states : Findings of the national trends and disparities in coronary heart disease, stroke, and other cardiovascular diseases in the united states. *Circulation, Journal of the American Heart Association*, 102:3137–3147, 2000.

[4] Jason M. Stevens and Gregory D. Buckner. Actuation and control strategies for miniature robotic surgical systems. *Journal of Dynamic Systems, Measurement, and Control*, Vol. 127 Issue 4:537–549, 2004.

[5] R.W. Bailey and J.L. Flowers. *Complications of Laparoscopic Surgery.* Quality Medical Publishing Inc, 2006.

[6] Michael Craven, Paul Ramphal, Daniel Coore, Brian Silvera, Maurice Fletcher, and Somara Newman. Design of an electromechanical pump system for training in beating heart cardiac surgers. *IEEE Proceedings, SoutheastCon 2002*, 2002.

[7] M.M. Black, T. Cochrane, P.J. Drury, and P.V. Lawford. A hydrodynamic model for the left side action of the human heart. *Annual International Conference of the IEEE Engineering in Medicine and Biology Society*, Vol. 12 No. 2, 1990.

[8] Gabriele Dubini, Riccardo Pietrabissa, and Roberto Fumero. Computational model role in designing circulation system simulators: An example. *Annual International Conference of the IEEE Engineering in Medicine and Biology Society*, Vol. 13 No. 5:2054–2055, 1991.

[9] Y.T. Chew, T.C. Chew, H.T. Low, and W.L. Lim. *Biomechanical Systems, Techniques and Applications Vol II, Cardovascular Techniques.* CRC Press LLC, 2001.

[10] David Elad, Shmuel Einav, and Myer Kutz (editor). *Standard Handbook of Biomedical Engineering and Design.* McGraw Hill, 2003.

[11] P.P. Chang, G.L. Matson, J.E. Kendrick, and V.C. Ridout. Parameter estimation in the canine cardiovascular system. *IEEE Transactions on Automatic Control*, AC-19 no. 6:927–931, 1974.

[12] Bruce E. Larock, Roland W. Jeppson, and Gary Z. Watters. *Hydraulics of Pipeline Systems*. CRC Press, 2000.

[13] Prof. Dr.-Ing. habil Bodo Heimann, Wilfried Gerth, and Karl Popp. *Mechatronik: Komponenten - Methoden - Beispiele*. Fachbuchverlag Leipzig im Carl Hanser Verlag, 2001.

[14] Jacob Goldstein, Rafael Beyar, and Samuel Sideman. Influence of pleural pressure variations on cardiovascular system dynamics, a model study. *Medical and Biological Engineering and Computing*, 26:251–259, 1988.

[15] BEI KIMCO Magnetics Division. *Voice Coil Actuators, An application guide*. BEI KIMCO, 804-A Rancheros Drive, San Morcos, CA 62069 U.S.A., 200x.

[16] J. David Bristow, Richard E. Ferguson, Fredric Mintz, and Elliot Rapaport. The influence of heart rate on left ventricular volume in dogs. *Journal of Clinical Investigation*, 42:649–655, 1963.

[17] Robert M. Payne, Hubert L. Stone, and Edward J. Engelken. Atrial function during volume loading. *Journal of Applied Physiology*, 31:326–331, 1971.

[18] J.P. Holt, E.A. Rhode, S.A. Peoples, and Helga Kines. Left ventricular function in mammals of greatly different size. *Circulation Research*, 10:798–806, 1962.

[19] Robert L. Hamlin, Wayne L. Klepinger, Kay W. Gilpin, and C. Roger Smith. Autonomic control of heart rate in the horse. *American Journal of Physiology*, 222:976–978, 1979.

[20] Lee Waite, Gabor Szabo, Charissa Bolind, and Christian Vahl. A lumped parameter model of ventricular filling: Pressure and flow waveforms. *Biomedical Sciences Instrumentation*, 36:75–80, 2000.

[21] Edward Chinchoy, Charles L. Soule, Andrew J. Houlton, William J. Gallagher, Mark A. Hjelle, Timothy G. Laske, Josée Morissette, and Paul A. Iaizzo. Isolated four-chamber working swine heart model. *The Annals of Thoracic Surgery*, 70:1607–14, 2000.

[22] BEI KIMCO Magnetics Division, Vista, CA 92081. *Linear Actuator, LA13-12-000-LTR*, 1994.

[23] Microchip Technology, Inc. *PIC18F2420/2520/4420/4520 Data Sheet (DS39631A)*, 2004.

[24] Motorola, Inc. *50 kPa On-Chip Temperature Compensated & Calibrated Silicon Pressure Sensors*, 2002.

[25] STMicroelectronics. *LM224A-LM324A Low Power Quad Operational Amplifier*, 2005.

[26] Infineon Technologies. *5-A H-Bridge for DC-Motor Applications*, 1999-10-07.

[27] Allan R. Hambley. *Electrical Engineering: Principles and Applications*. Prentice Hall, Upper Saddle River, New Jersey 07458, 1997.

[28] STMicroelectronics. *M54HCT02-M74HCT02 Quad 2-Input NOR Gate*, 1993.

[29] Dogan Ibrahim. *Microcontroller Based Applied Digital Control*. Wiley, 2006.

Appendices

A Units and constants

Table 4: Constants used in system modeling

Parameter	*Units*	*Description*
α	kg/m^7	fluid resistance
α'	$\frac{kg}{m^4 s}$	linear fluid resistance
β	kg/m^4	fluid inertance
γ	$\frac{m^5}{N}$	compliance
k_f	$\frac{N}{A}$	voice coil force constant
k_b	$\frac{Volt\ s}{m}$	voice coil back EMF constant
R	Ohm	voice coil resistance
L	Henry	voice coil inductance
L	m	length of conduit
A	m^2	pump displacement relation
b	Ns/m	linear friction coefficient
k	$\frac{N}{m}$	diaphragm stiffness
k_s	m	screw equivalence coefficient
k_t	$\frac{N}{A}$	DC motor torque constant
J	Nms^2	rotor moment of inertia
B	Nms	bearing friction coefficient
m	kg	VCA moving mass
c	Ns/m	VCA friction coefficient

B Microcontroller C code

The following *C* source code implements a discrete PID controller on a Microchip 18F4520 (it would work with some modification on the older 18F452; namely, the ADC routine would need to be modified).

The code assumes that the amplified sensor input is connected to pin three (AN1), while the PWM output is pin 17 (CCP1). The H-bridge polarity output is pin 18 (RC3).

```
/*
FILE: gearpumpPID.c
AUTHOR: Sean P.M. Dugan
DESCRIPTION: This code implements a discrete PID controller to control a
12V gear pump. The gear pump is commanded to follow a triangular velocity
trajectory from a low pressure P_dia to a high pressure P_sys.

The code was developed using the Microchip C18 compiler.
*/

#include <p18f4520.h>
#include <timers.h>
#include <adc.h>
#include <pwm.h>
#include <delays.h>
#include <math.h>

#define abs(x) ((x<0)?(x*-1):(x))

void timer_ISR (void);
void high_ISR (void);

static int ADCresult;

/*Command and error signal histories.*/
float uk;
float uk_1;
float ek;
float ek_1;
float ek_2;

float yk_1;
float yk_2;
```

```
/*Sampling rate:*/
float dT = 0.01306;

/*Discrete system parameters.*/
float a1 = 9.7958;
float a2 =-11.5934;
float a3 = 2.1304;

/*Desired decay rate and stiffening factors:*/
float sigma = 4;
float lambda = 0.1;

/*Discrete PID gains */
float c1 = -2.9635;
float c2 = 10.9303;
float c3 =  -7.9599;
/*[a,dt]=figparameterestimationLSQ244(1,0)
C = GetPIDCGains(a,.1,4,0.01306)*/

/*The counter serves as the system "clock". Each increment represents T
seconds, where T is the sampling/interrupt interval.*/
unsigned long counter;
int  Pdia = 300;
int  Psys = 550;

/*Triangle velocity interval lengths in counter units.*/
double Ts = 400;
double Th = 0;
double Td = 400;
double Tl = 0;

/*Maximum velocity and accelerations.*/
double Vs;
double Vd;
double as;
double ad;

int GetADC(PARAM_SCLASS unsigned char channel);
int GetInput(void);
int GetSetPoint(void);
```

```
/*Interrupt vector.*/
#pragma code low_vector = 0x18
void low_interrupt (void)
{
    _asm
        GOTO timer_ISR
    _endasm
}

/*The interrupt function. It is executed each time timer0 overflows
(the sampling interval). The execution follows the flow chart discussed
in section 7.*/
#pragma code
#pragma interruptlow timer_ISR
void timer_ISR (void)
{
    int yd;
    int yk;
    float alpha = 0.05;
    PORTBbits.RB0=1;

    INTCONbits.TMR0IF = 0;

    if(PORTAbits.RA4 == 0)
    {
        yd  = GetSetPoint();
        yk  = GetADC(ADC_CH1);
        yk = alpha*yk_1+(1-alpha)*yk;// + (yk_1-yk_2)*alpha;
        ek  = yd - yk;
        uk  = GetInput();
        if(uk>0)
        {
            SetDCPWM1(abs(uk));
            PORTCbits.RC3 = 1;
        }
        else
        {
            SetDCPWM1(abs(uk));
            PORTCbits.RC3 = 0;
        }
```

```
        ek_2 = ek_1;
        ek_1 = ek;
        uk_1 = uk;
        yk_2 = yk_1;
        yk_1 = yk;
    }else if(PORTAbits.RA4 == 1)
    {
        if(PORTCbits.RC4 == 0)
        {
            PORTCbits.RC3 = 1;
            SetDCPWM1(244);
            PORTCbits.RC4 = 0;
        }else
            SetDCPWM1(0);
    }

    PORTBbits.RB0=0;
}

void main (void)
{
    /*Initialize all of the variables used by the control algorithm.*/
    counter  = 0;
    ek       = 0;
    ek_1     = 0;
    ek_2     = 0;
    uk       = 0;
    uk_1     = 0;
    yk_1    = 0;
    yk_2    = 0;

    /*Calculate the maximum systolic and diastolic pressure velocity and
accelerations.*/
    Vs = 2*(Psys-Pdia)/Ts;
    Vd = 2*(Pdia-Psys)/Td;
    as = Vs/(Ts/2);
    ad = Vd/(Td/2);

    /*Blink an LED to make sure the thing is working (attached to pin
33).*/
    TRISBbits.TRISB0 = 0;
```

```
    PORTBbits.RB0 = 0;

    TRISAbits.TRISA4 = 1;
    /*If C4 is high, execute the step input instead of the control sequence.*/
    TRISCbits.TRISC4 = 1;

    /*Set the timer to overflow every 13ms with a 10MHz crystal.*/
    OpenTimer0(TIMER_INT_ON & T0_8BIT & T0_SOURCE_INT & T0_PS_1_128);

    TRISCbits.TRISC2 = 0; /*PWM signal*/
    TRISCbits.TRISC3 = 0; /*DIR signal*/
    T3CON = 0x81;

    /*Configure the PWM module.  Use as low a frequency as possible or
the motor will wake up your dog.*/
    OpenTimer2(TIMER_INT_OFF & T2_PS_1_16 & T2_POST_1_1);
    OpenPWM1(0xFF);
    SetDCPWM1(0);
    PORTCbits.RC3 = 1;

    /*Enable the ADC on channel 1.*/
    OpenADC(ADC_FOSC_16 & ADC_RIGHT_JUST & ADC_12_TAD, ADC_CH1 &
ADC_INT_OFF, 0);
    ADCON1 = 0x00;

    /*Enable the interrupts... And away we go!*/
    RCONbits.IPEN   = 1; /*enable interrupt priority scheme*/
    INTCONbits.GIEL = 1; /*enable low interrupts*/
    INTCONbits.GIEH = 1; /*enable global interrupts*/

    while(1)
    {
        /* Do nothing.  Forever.  The saddest snippet of C code ever writ-
ten.*/
    }
}

int GetADC(PARAM_SCLASS unsigned char channel)
{
    union ADCResult i;
    #ifdef ADC_INTERFACE_OLD
```

```
        ADCON0 = (channel & 0b00111000) |(ADCON0  & 0b11000111);
    #else
        ADCON0 = ((channel >> 1) & 0b00111100) |(ADCON0  & 0b11000011);
    #endif
     ADCON0bits.GO = 1;
    while(ADCON0bits.GO);
    i.br[0] = ADRESL;
    i.br[1] = ADRESH;
    return (i.lr);
}

int GetInput(void)
{
    int uk;
    /*The discrete PID control rule:*/
    uk = uk_1 + c1*ek + c2*ek_1 + c3*ek_2;

    /*Don't let the value exceed the maximum PWM value of 2^10-1.*/
    if(uk>1023)
        uk = 1023;
    if(uk<-1023)
        uk = -1023;
    return uk;
}

int GetSetPoint(void)
{
    float y;
    int t;

    /*Reset the counter if an entire pumping cycle has elapsed.*/
    if(counter==Ts+Td+Th+Tl)
    {
        counter = 0;
    }

    /*The time needs to be shifted back to facilitate integration of the velocity curve, and we don't want to disrupt the counter.*/
    t = counter;

    if(t<Ts/2)
```

```
    {
        y = as*t*t/2 + Pdia;

    }else if(t>=Ts/2 && t<Ts)
    {
        t = t-Ts/2;
        y = Vs*t-as/2*t*t+Pdia+(Psys-Pdia)/2;

    }else if(t>=Ts && t<Ts+Th)
    {
        y = Psys;

    }else if(t>=Ts+Th && t<Ts+Th+Td/2)
    {
        t = t-Ts-Th;
        y = ad/2*t*t + Psys;

    }else if(t>=Ts+Th+Td/2 && t<Ts+Th+Td)
    {
        t = t-Ts-Th-Td/2;
        y = Vd*t - ad/2*t*t + Pdia +(Psys-Pdia)/2;

    }else
    {
        y = Pdia;
    }
    counter++;
    return y;
}
```

C Parameter fitting with the least squares method

In principle it would be possible to calculate the system parameters φ_i and ϑ_i from known or measured constituent quantities (such as the diaphragm stiffness k or fluid resistance α), however, some factors, such as the screw equivalence factor k_s are not directly measurable. It is more accurate and convenient to perform system identification experiments to determine the discretized system parameters a_i directly by applying a known input to the system, measuring the response, and then fitting the resulting data to the model using the least squares method.

At time step $k = 1$, Eq.3.40 may be expressed in the equivalent matrix form as

$$\mathbf{y}_1^T \mathbf{a} = u_{-1}$$

Written explicitly,

$$\begin{bmatrix} y_1 & y_0 & y_{-1} \end{bmatrix} \begin{bmatrix} a_1 \\ a_2 \\ a_3 \end{bmatrix} = \begin{bmatrix} u_{-1} \end{bmatrix} \tag{.1}$$

For each subsequent time step, Eq..1 may be augmented progressively up to time step $k = N$ following the pattern

$$\begin{bmatrix} y_1 & y_0 & y_{-1} \\ y_2 & y_1 & y_0 \\ y_3 & y_2 & y_1 \\ y_4 & y_3 & y_2 \\ & \vdots & \\ y_N & y_{N-1} & y_{N-2} \end{bmatrix} \begin{bmatrix} a_1 \\ a_2 \\ a_3 \end{bmatrix} = \begin{bmatrix} u_{-1} \\ u_0 \\ u_1 \\ u_2 \\ \vdots \\ u_{N-2} \end{bmatrix} \tag{.2}$$

The result is a matrix equation of the form $\mathbf{Ya} = \mathbf{u}$. The vector $\mathbf{a}$ that minimizes the squared error $\mathbf{e}^T\mathbf{e} := (\mathbf{Ya} - \mathbf{u})^T(\mathbf{Ya} - \mathbf{u})$ is found by taking the derivative of $\mathbf{e}^T\mathbf{e}$ with respect to $\mathbf{a}$, setting the result equal to zero, and solving for $\mathbf{a}$. This yields the familiar least squares solution

$$\mathbf{a} = \left(\mathbf{Y}^T\mathbf{Y}\right)^{-1}\mathbf{Y}^T\mathbf{u} \tag{.3}$$

To find the system parameters, N measurements of the system are made as a known input is applied. As the matrix $\mathbf{Y}$ is formed, the values of y_k for $k = -1$ and $k = 0$ would be set to y_1 (assuming the system is in equilibrium when the experiment begins). For the input, $u_{-1} = u_0 = 0$.